

1 This manuscript is a non-peer reviewed pre-print submitted to EarthArXiv.

2 **Global air quality change during COVID-19: a synthetic result of human activities**  
3 **and meteorology**

4 **Qianqian Yang<sup>1,\*</sup>, Bin Wang<sup>1,\*</sup>, Yuan Wang<sup>1,\*</sup>, Qiangqiang Yuan<sup>1,\*</sup>, Caiyi Jin<sup>1</sup>, Jiwen**  
5 **Wang<sup>1</sup>, Shuwen Li<sup>1</sup>, Muyu Li<sup>1</sup>, Tongwen Li<sup>2, †</sup>, Song Liu<sup>3</sup>, Huanfeng Shen<sup>2</sup>, Liangpei**  
6 **Zhang<sup>4</sup>**

7 <sup>1</sup> School of Geodesy and Geomatics, Wuhan University, Wuhan, China.

8 <sup>2</sup> School of Resource and Environmental Sciences, Wuhan University, Wuhan, China.

9 <sup>3</sup> Deutsches Zentrum für Luft- und Raumfahrt (DLR), Institut für Methodik der Fernerkundung  
10 (IMF), Oberpfaffenhofen, Germany

11 <sup>4</sup> State Key Laboratory of Information Engineering in Surveying, Mapping and Remote Sensing,  
12 Wuhan University, Wuhan, China.

13 Corresponding author: Qiangqiang Yuan ([qqyuan@sgg.whu.edu.cn](mailto:qqyuan@sgg.whu.edu.cn)).

14 \*These authors contributed equally: Qianqian Yang, Bin Wang, Yuan Wang, Qiangqiang Yuan.

15 †Present address: School of Geospatial Engineering and Science, Sun Yat-Sen University,  
16 Guangzhou, China

17

## 18 **Abstract**

19 In recent months, coronavirus disease 2019 (COVID-19) has been spreading around the globe,  
20 and this has led to a rare reduction in human activities. In such a background, data from ground-  
21 based environmental stations, satellites, and reanalysis materials are utilized to conduct a  
22 comprehensive analysis of the air quality changes during the COVID-19 outbreak at the global  
23 scale. The results showed that under the impact of the COVID-19 outbreak, a significant decrease  
24 in particulate matter (PM<sub>x</sub>) and nitrogen dioxide (NO<sub>2</sub>) occurred in more than 40% of the world's  
25 land area, with NO<sub>2</sub> decreasing by approximately 30% and PM<sub>x</sub> decreasing approximately 20%. In  
26 addition, the mobility, meteorological factors, and the response speed to COVID-19 outbreaks in  
27 cities were examined, and it was further found that in quick-response cities, lockdowns produced a  
28 sharp decline in mobility in a short time. This had a large impact on air quality. In contrast, in slow-  
29 response cities, declines in mobility occurred beginning with the confirmation of the first COVID-  
30 19 case (FCC) and dropped gradually for a relatively long period. The impact of the FCC,  
31 lockdowns, and meteorological factors on air quality can be comparable.

32 **Keywords:** Air quality, COVID-19, Lockdown, First case confirmation

## 33 **Introduction**

34 During the past several decades, worldwide monitoring has provided concrete evidence that  
35 human activities, such as fossil fuel combustion (vehicles and factories), industrial production,  
36 construction activities, biomass burning, and changes in land use, are causing serious pollution  
37 problems in the atmosphere<sup>1,2</sup>. Air pollution is a major environmental risk to human health<sup>3,4</sup>.  
38 According to a report by the World Health Organization (WHO), nearly 91% of the world's  
39 population lives in places where the air quality levels exceed WHO limits, and ambient air pollution  
40 accounts for an estimated 4.2 million deaths per year<sup>5</sup>. With air pollution exerting heavy pressure  
41 on the environment, scientists around the world have conducted a large number of studies that  
42 explore how to reduce air pollution by making human activities cleaner and greener<sup>6</sup>. However,

43 there has seldom been a chance to directly observe how such changes will affect the global air  
44 quality.

45 The coronavirus disease 2019 (COVID-19)<sup>7-9</sup>, which has had successive outbreaks in cities  
46 around the world<sup>10-12</sup>, has caused unprecedented suffering<sup>13-16</sup>. As of May 23, 2020, the COVID-19  
47 pandemic has caused more than 5.2 million infections and 340,477 deaths in the world<sup>17</sup>. People  
48 around the world have started to change their usual lifestyles to reduce the risk of infection, and  
49 countries and regions have begun to adopt various restriction measures to slow down the spread of  
50 the novel coronavirus<sup>18,19</sup>. People have been staying at home, cars have been idle in garages, planes  
51 have been parked in parking aprons, and some factories have been forced to close. Hence, there has  
52 been a rare large-scale slowdown of human activities all over the world. How the global air quality  
53 will change under such a situation remains an interesting question<sup>20-22</sup>.

54 Currently, there are a number of studies researching the impact of the lockdowns on air quality  
55 changes<sup>23-34</sup>. While most of the studies are either confined to local regions<sup>23-27</sup> or certain types of  
56 air pollutants<sup>27-30</sup>, there are some studies analyzing the air quality changes at the global scale and  
57 from a synthetic perspective<sup>32-34</sup>. However, there are still several limitations of these global studies.  
58 First, the current studies have concentrated on the impact of the lockdowns on air quality. COVID-  
59 19 affects human activities not only through lockdowns, but also in other aspects, such as the  
60 confirmation of the first COVID-19 case (FCC). The news of the first case confirmation may worry  
61 some residents and reduce their activities. Therefore, the impact of FCC on air quality should also  
62 be considered and evaluated. Second, most of the current studies have analyzed air quality changes  
63 during the COVID-19 period by simply calculating the differentials during a short period, which  
64 can be direct and intuitive, but it also could contain large uncertainties. Multiple time series analysis  
65 methods should be explored and adopted to obtain a more reliable conclusion. Finally, a combined  
66 analysis of air quality changes and mobility and meteorological changes is still lacking. Hence, a

67 comprehensive understanding of air quality changes during the COVID-19 outbreak at the global  
68 scale is still urgently required.

69 In this study, the air quality changes during the time since the COVID-19 outbreak began are  
70 investigated at the global scale. In addition, the impacts of the FCCs and lockdowns on air quality  
71 are investigated using satellite products, reanalysis data, and station measurements, and these data  
72 are analyzed in relationship to mobility changes and meteorology variations. A workflow schematic  
73 of this study is shown in Figure S1. For more details about the methods and materials, please refer  
74 to the experimental procedures and supplemental experimental procedures.

## 75 **Results**

### 76 **Global air quality changes during COVID-19**

77 The variation trends of global pollutants anomalies (methods and materials) detected using the  
78 Mann-Kendall (MK) test are depicted in Figure 1. The anomalies of PM<sub>2.5</sub>, PM<sub>10</sub>, and NO<sub>2</sub>  
79 significantly declined in general, while the other pollutants showed an uptrend or insignificant trend.  
80 Specifically, the percentages of areas showing significant downtrends (uptrends) during the  
81 COVID-19 epidemic were 42.32% (1.49%), 40.32% (1.21%), and 45.26% (9.52%) for the PM<sub>2.5</sub>,  
82 PM<sub>10</sub>, and NO<sub>2</sub> anomalies, respectively. This result is consistent with the conclusion of Venter et  
83 al.<sup>32</sup>, although they researched the global change in PM<sub>2.5</sub>, O<sub>3</sub>, and NO<sub>2</sub> primarily based on ground  
84 station data. However, for the O<sub>3</sub>, SO<sub>2</sub> and CO anomalies, the percentages were 30.45% (15.88%),  
85 23.15% (12.68%), and 30.15% (16.07%), respectively. The spatial distribution of the regions where  
86 air quality improved varied with the pollutant types. Regions where PM<sub>2.5</sub> declined significantly  
87 were primarily located in the northern hemisphere and eastern Australia. The spatial distribution of  
88 the PM<sub>10</sub> variation trend was similar to that of PM<sub>2.5</sub> in most areas. However, an exception occurred  
89 in a small region of the northern Qinghai-Tibet Plateau, which is on the edge of the Taklamakan  
90 Desert. The v-component of wind (VWS) remained negative in the northern Qinghai-Tibet Plateau  
91 from January 2020 to March 2020 (Figure S2), and the anomalies of the VWS were also negative

92 (Figure 2), which suggested that a southern wind was prevailing and stronger than in previous years  
93 in this area. Therefore, affected by wind, the particulate matter was transported from the desert to  
94 the south and accumulated at the northern Qinghai-Tibet Plateau because of the topography. PM<sub>10</sub>  
95 accounted for the majority of pollution in the desert<sup>35</sup>, so the impact on PM<sub>2.5</sub> was not as significant  
96 as PM<sub>10</sub>, so the variation trends of PM<sub>2.5</sub> and PM<sub>10</sub> were different. NO<sub>2</sub> anomalies declined in most  
97 areas except for near the Arctic Circle. O<sub>3</sub> anomalies decreased significantly in the U.S., Canada,  
98 and northern Africa, but they increased in regions around the equator, possibly because of the  
99 stronger solar radiation and higher temperatures there, which can promote photochemical reactions  
100 and thus produce more O<sub>3</sub><sup>36</sup>. However, anomalies of SO<sub>2</sub> and CO showed increases or  
101 nonsignificant trends across the world. In addition, it is worth noting that the positive trends of four  
102 gas pollutants in the polar region (Figure 1C-F) might be inaccurate due to the great number of  
103 missing values here, which does not affect the discovery and conclusion for other areas. To  
104 demonstrate the detailed variations in air quality and their relationship with human activities, China,  
105 Europe, the Contiguous United States (CONUS), and Brazil (Figure S3) were focused on, where  
106 COVID-19 was the most prevalent<sup>12,16,37</sup>.

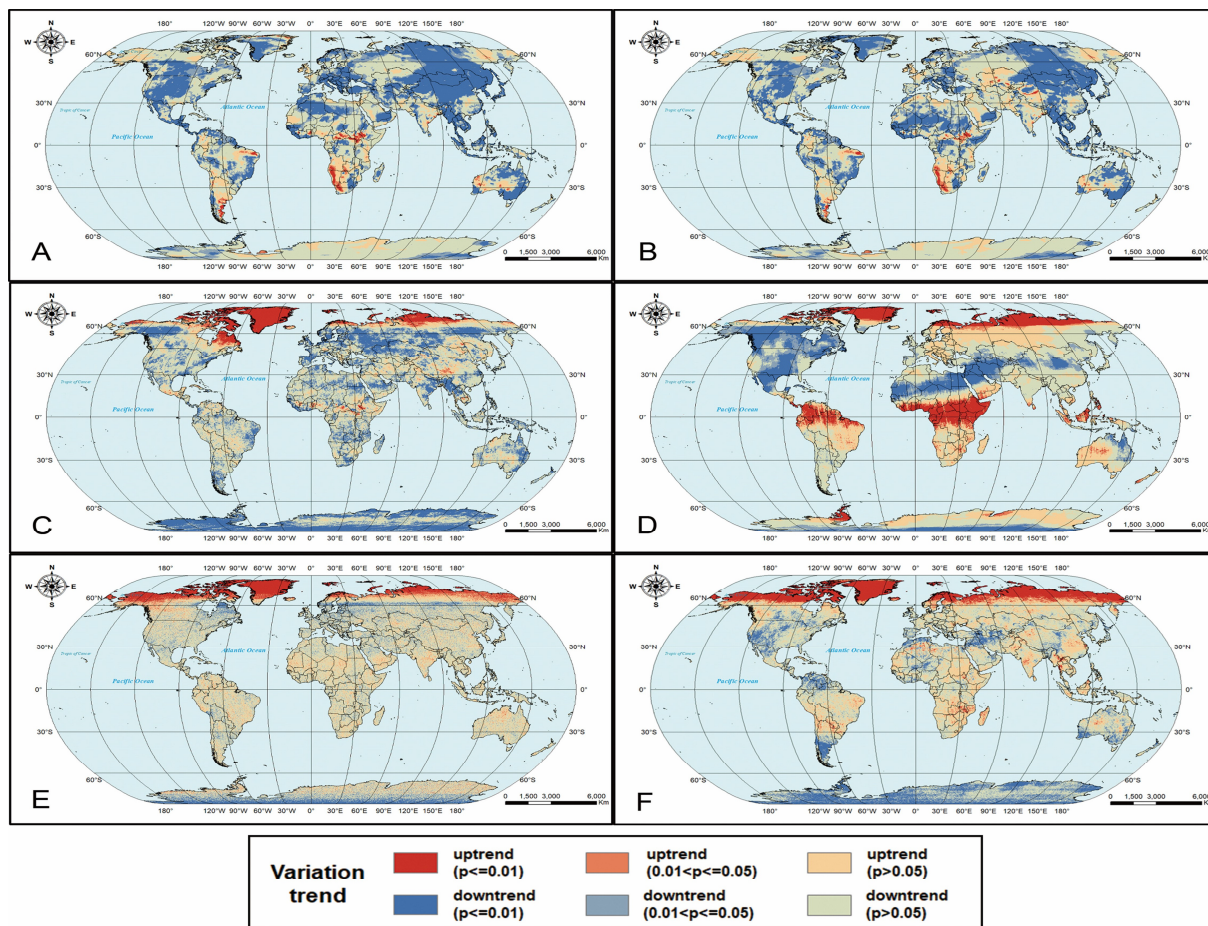


**Figure 1.** Variation trends and the significance of six pollutant anomalies. The trends and significances of all of the pollutants were calculated using the MK test. A-F represent the global distribution of the results of anomalies in PM<sub>2.5</sub>, PM<sub>10</sub>, NO<sub>2</sub>, O<sub>3</sub>, SO<sub>2</sub>, and CO, respectively.

PM<sub>2.5</sub> and PM<sub>10</sub> (PM<sub>x</sub>) anomalies decreased significantly in northwestern China, central and northeastern CONUS, and most parts in Europe and Brazil. The PM<sub>x</sub> anomalies remained negative in most regions of China during COVID-19. While in Europe, the signs of PM<sub>2.5</sub> anomalies did not display a uniform pattern prior to week four, and then the values remained negative in most areas until week 12 (Figure S4). Although there were no compulsory measures declared by the local governments then, it was inferred that people were likely to spontaneously reduce their outing activities after the COVID-19 pandemic began to be prevalent. Therefore, this caused a decline in PM<sub>2.5</sub>. The trend in the anomalies of PM<sub>10</sub> was similar to PM<sub>2.5</sub> in most areas of Europe, except the Southwest portion (Figure S5). In the northeastern CONUS, the anomalies of PM<sub>2.5</sub> were negative

120 in week 11. This was close to the time (March 19, 2020) that the number of CONUS cases exceeded  
121 10,000, and 40% of them were in New York State. The spatiotemporal pattern of the anomalies of  
122 PM<sub>x</sub> and CO in Brazil were similar. Both of these pollutants decreased in most of the area, but they  
123 were unexpectedly increased in the eastern coastal area and in the countries southwest of Brazil.  
124 Figure 2C shows that the zonal wind (UWS, positive represent eastward wind) in the eastern coastal  
125 areas of Brazil showed positive anomalies. Considering that westward wind prevails in eastern  
126 Brazil from January to March, the positive UWS anomalies could have indicated a decrease in the  
127 westward wind speed, which were likely to lead to an accumulation of pollutants. Therefore, the  
128 anomalies of PM<sub>x</sub> concentration showed an uptrend in the east with time. For other regions in Brazil  
129 where the meteorological data did not significantly change, the concentration of PM<sub>x</sub> still declined  
130 under the impact of the COVID-19 lockdown. As for the PM<sub>x</sub> and CO increases in the countries  
131 southwest of Brazil, it was inferred this might have been a result of increased wildfires. These areas  
132 witnessed an increase in wildfire frequency in 2020 compared with 2019, especially since March  
133 (Figure S6), thus leading to an increase in PM<sub>x</sub> and CO.

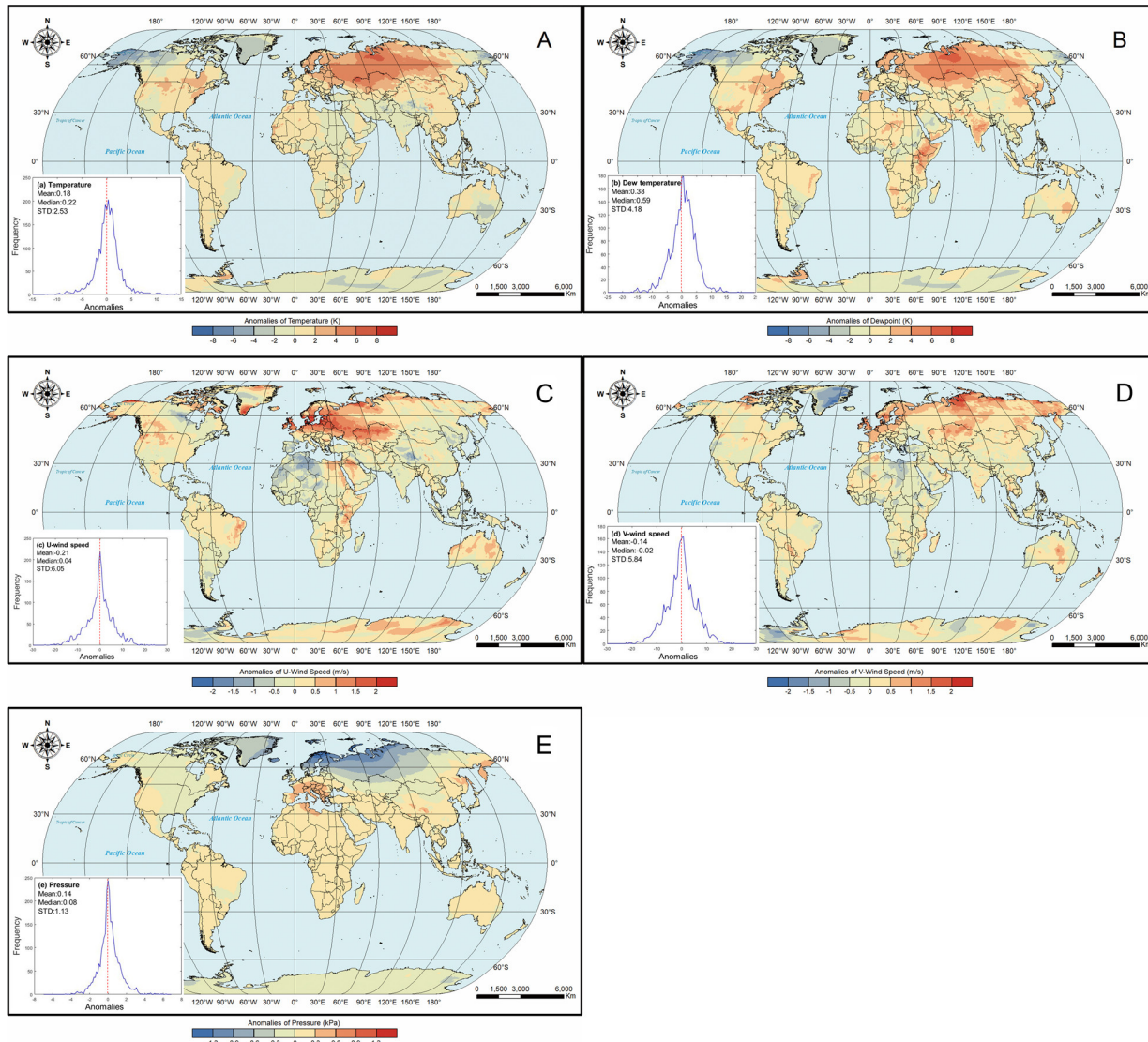


**Figure 2.** The average anomalies from January to April 2020 of six meteorological factors. The baseline for the anomalies is the average meteorological conditions for the same period during 2017–2019. A-F represent the anomalies for temperature (TEM), dewpoint temperature (DEW), zonal wind (UWS), meridional wind (VWS), and pressure (PS), respectively. The probability distribution plot in the bottom left corner of each subfigure shows the frequency distribution of the meteorological anomalies in the 26 studied cities.

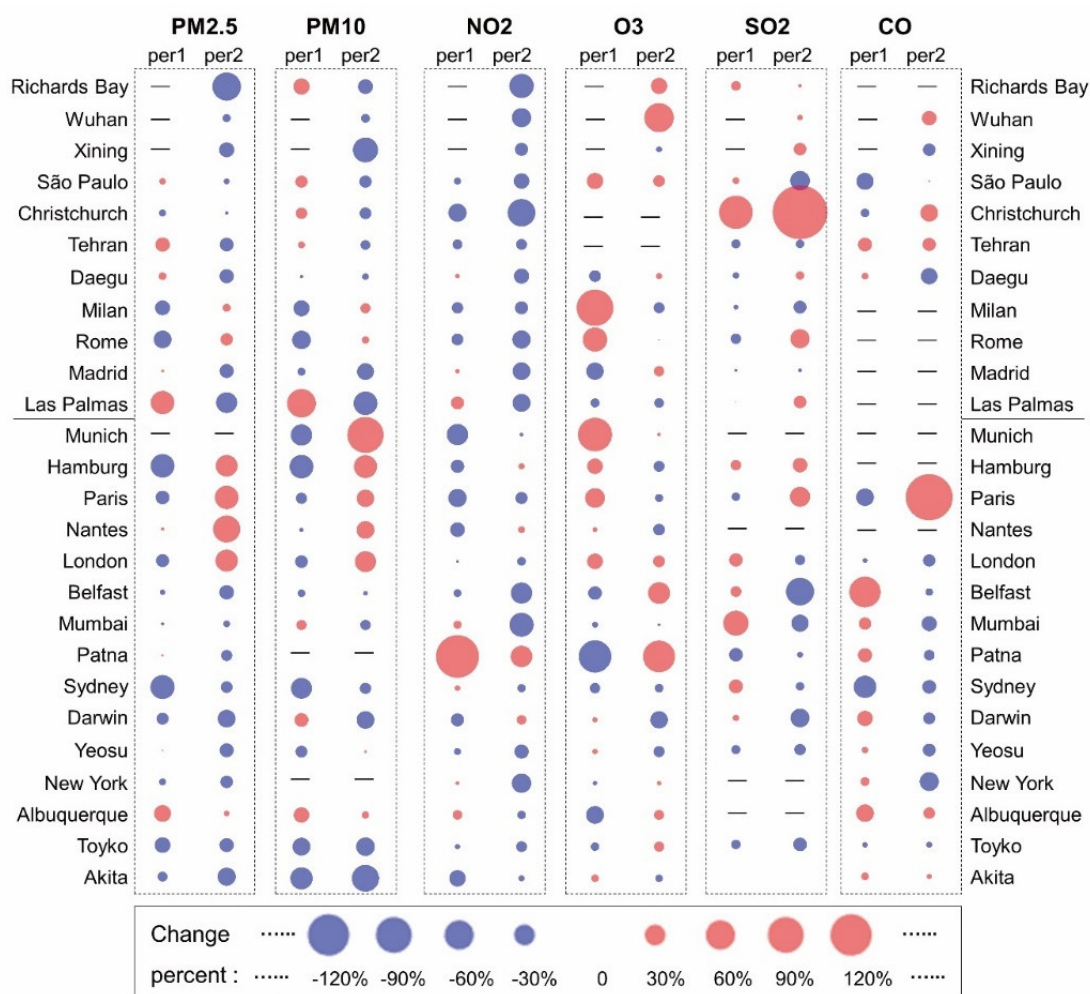
For  $\text{NO}_2$ , the anomalies primarily had a significant downward trend in central and northern China (Figures S3 and S7), which was most probably related to the restrictive measures issued by the government<sup>38</sup>. Specifically, the anomalies experienced a -129% fractional change after

144 lockdown started, which was consistent with the conclusion of Le et al. They calculated a change  
145 percentage based on data from 2019 to 2020 of -71.9%<sup>39</sup>. The anomalies of NO<sub>2</sub> typically fluctuated  
146 in central and eastern China prior to the outbreak of COVID-19 (Figure S7). During the lockdown  
147 period which started on January 23, 2020 in Wuhan, the NO<sub>2</sub> anomalies remained negative in most  
148 areas of central and eastern China until week 12. The next week, due to work resumptions, the  
149 anomalies of NO<sub>2</sub> turned positive. Compared to China, the timing of the changes in the NO<sub>2</sub>  
150 anomalies in Europe showed a certain delay due to the difference in the COVID-19 outbreak time  
151 (Figure S7). The anomalies of NO<sub>2</sub> turned negative in most areas after week 11 when the local  
152 governments declared their restrictions to deal with the COVID-19 epidemic. In the eastern  
153 CONUS, the values turned negative in week eight. Although the values fluctuated in week 12 in  
154 some areas, they remained negative in areas with severe epidemic, such as New York. The  
155 anomalies in NO<sub>2</sub> showed a significant downtrend in urban areas in east Brazil. However, the  
156 concentration of NO<sub>2</sub> in Brazil were less serious than in the other three places, so the weekly  
157 variations in the anomalies (Figure S7) were unobvious from a satellite perspective relative to other  
158 regions.

159 For the other three pollutants, the variation trends were not as significant as PM<sub>x</sub> and NO<sub>2</sub>, but  
160 the turning points of the time series were related to the COVID-19 lockdown time. The turning  
161 point of the O<sub>3</sub> anomalies in the CONUS was observed at the 11<sup>th</sup> week, and the anomalies of SO<sub>2</sub>  
162 and CO also turned at approximately week 12, all close to the lockdown time in the CONUS. The  
163 turning point of the SO<sub>2</sub> anomalies in Europe was week nine, which was near to most of the  
164 European countries lockdown times. As demonstrated above, the satellite and reanalysis data  
165 showed that the global air quality significantly improved during COVID-19, and the turning points  
166 of pollutants variations were closely related to lockdown times.

### 167 **Ground-based air quality changes in typical cities**

168 Satellite and reanalysis data can monitor air quality changes over a large extent with relatively  
169 continuous spatial coverage. However, the results may not be able to exactly reflect near-surface  
170 pollution variations. Therefore, 26 typical cities were selected and ground-based monitoring data  
171 were utilized for further analysis. There were different lockdown periods in different countries and  
172 cities, thus a study period was chosen that covered most of the important time nodes in these cities  
173 (e.g., the FCC and lockdown). Specifically, the study period was from January 1, 2020 to April 24,  
174 2020, and the distribution of cities and the time nodes of each are shown in Figure S8. The cities  
175 were divided into two groups according to the time difference between the FCC and the lockdown.  
176 Cities with a time difference of fewer than 50 days (for more information about the determination  
177 of the threshold, please refer to Figure S9) were defined as quick-response cities (11 out of 26 cities).  
178 The others were defined as slow-response cities (15 out of 26 cities). For each city, the change  
179 curves of the daily air quality index (AQI, for more information, please refer to experimental  
180 procedures section) during the study period are displayed in Figure S10, and the change percentage  
181 since the FCC or lockdown are shown in Figure 3 and Table S1. The results indicated that for PM<sub>2.5</sub>,  
182 PM<sub>10</sub>, and NO<sub>2</sub>, most of the cities showed an obvious decreasing trend, which agrees with many of  
183 the current studies<sup>25,26,28-32</sup>. One of the common sources of PM<sub>2.5</sub>, PM<sub>10</sub>, and NO<sub>2</sub> is vehicle exhaust  
184 emissions. The transportation density during the COVID-19 outbreak largely decreased (Figure  
185 S11), directly leading to a decline in vehicle exhaust emissions and the AQIs of PM<sub>2.5</sub>, PM<sub>10</sub>, and  
186 NO<sub>2</sub>. In addition, O<sub>3</sub> and CO also decreased during the study period, but in most cases, the declines  
187 were insignificant ( $p>0.05$ ). The change in SO<sub>2</sub> was insignificant ( $p>0.05$ ), as well for most of the  
188 cities, with an insignificant decrease prior to lockdown, and an insignificant increase after the FCC.  
189 In general, the results from the ground-based observations were similar to those of the satellite and  
190 reanalysis material.



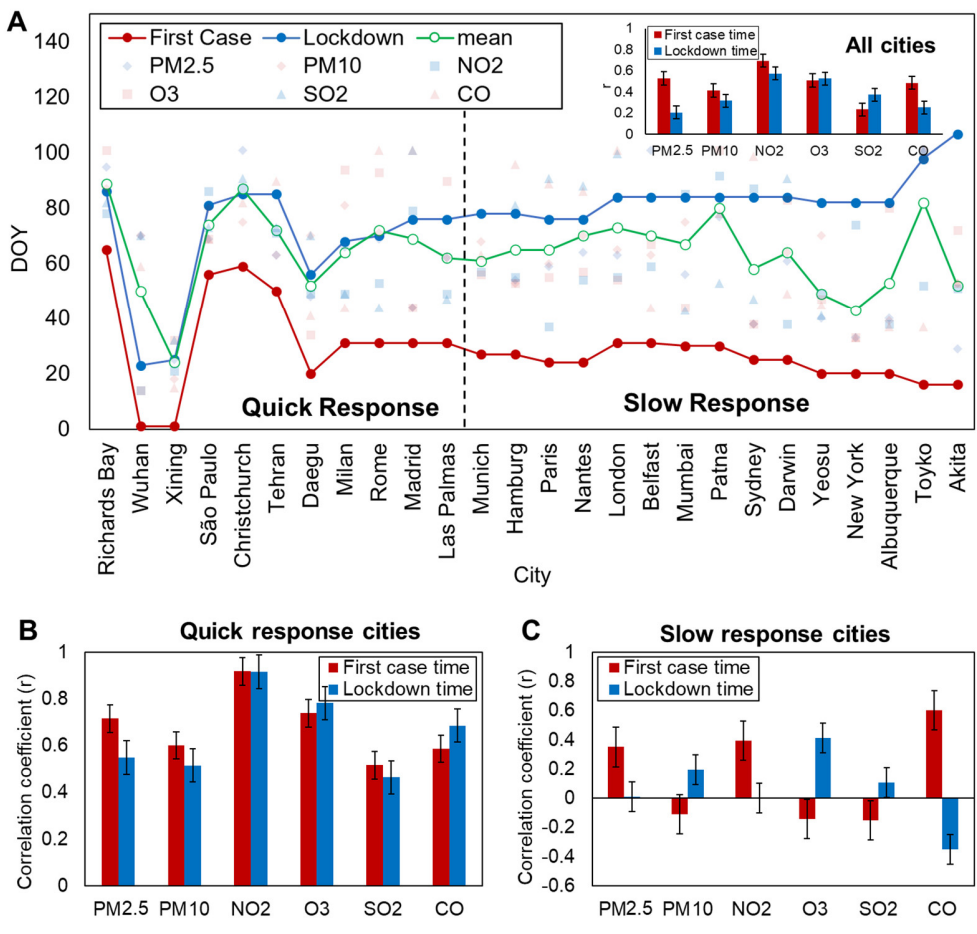
191

192 **Figure 3.** The percentage change in the AQI after FCC/lockdown (per1/per2) for six pollutants in  
 193 26 cities. The blue (red) circles indicate a decrease (increase) in the AQI, the larger the circle, the  
 194 greater the AQI decrease/increase. The dash lines in the rectangles stand for missing data. Cities  
 195 above the black lines are the quick-response cities and below the lines are the slow-response cities.

196 **Correlation between the FCC\lockdown and air quality changes**

197 The satellite and reanalysis data revealed the relationships between air quality changes and  
 198 human activity slowdowns caused by the COVID-19 pandemic. Ground-based data were used to  
 199 quantify these relationships. The time when the daily air quality anomalies began to change  
 200 (referred to as the change point hereafter) was detected using a time series analysis approach. The  
 201 results showed that these change points were highly correlated with the time of the FCC/lockdowns  
 202 (Figure 4A and Table S2). Generally, the change point of NO<sub>2</sub> had the highest correlation with the

203 FCC/lockdown time, with correlation coefficients,  $r$ , of 0.69 ( $p < 0.05$ ) and 0.58 ( $p < 0.05$ ),  
 204 respectively.  $O_3$  had  $r$  of 0.56 ( $p < 0.05$ ) and 0.51 ( $p < 0.05$ ) for lockdown time and the FCC time,  
 205 respectively. In addition, the change point of the  $PM_{2.5}$  AQI anomalies had a high correlation with  
 206 the time of the FCC ( $r = 0.53$ ,  $p < 0.05$ ), but it had a relatively low correlation ( $r = 0.26$ ,  $p = 0.21$ ) with  
 207 the lockdown time. The  $r$  values for the other three pollutants ranged from 0.23 to 0.48.



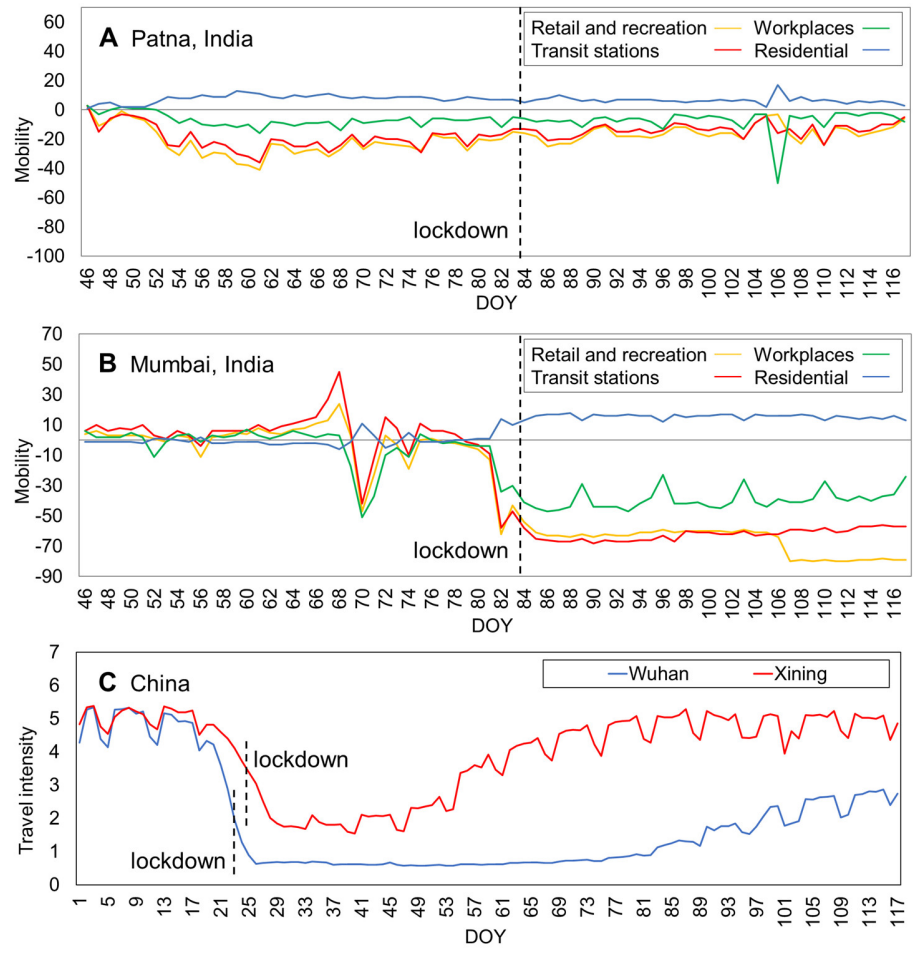
209 **Figure 4.** The relationship between the change point in the time series and the time of the  
 210 FCC/lockdown. (A) The detected change point times and the FCC/lockdown times in the 26 cities.  
 211 DOY represents the day of year. The green line is the mean times of the change points of the six  
 212 pollutants. The histogram in the upright corner displays the correlation between them. (B) The  
 213 correlations between the change point times and the FCC/lockdown times in the quick-response  
 214 cities and (C) in the slow-response cities.

215 A comparison was also conducted between the quick- and slow-response cities. In the quick-  
216 response cities, the change points were very close to the lockdown time and then got closer to the  
217 FCC time in slow-response cities (Figure 4A). In addition, in the quick-response cities, the  
218 correlations between the change points and the FCC/lockdown times ( $r$  ranges from 0.48 to 0.92)  
219 were much higher than that in the slow-response cities ( $r$  ranges from -0.38 to 0.58) (Figure 4B, C).  
220 COVID-19 caused air quality changes primarily due to alterations in human activities. When a city  
221 made a quick response to the COVID-19 pandemic, social activities and human behaviors changed  
222 drastically in a short time due to the restrictions. Therefore, changes in human activities caused by  
223 the lockdown became the dominant factor affecting air quality, which explains the high consistency  
224 between the change points in air quality and the lockdown times. In contrast, in the slow-response  
225 cities, human activities changed gradually over a long period of time, urged either by the fear of  
226 being infected when the first case appeared or due to government restrictions. During this period,  
227 the influencing factors of air quality were not dominated by lockdown anymore, and the impact of  
228 lockdown, the FCC, and meteorological factors could be comparable. This could be the reason for  
229 the poor correlations between air quality change points and the lockdown/FCC times in the slow-  
230 response cities.

### 231 **Quantification of the impact of the FCC and lockdowns on air quality**

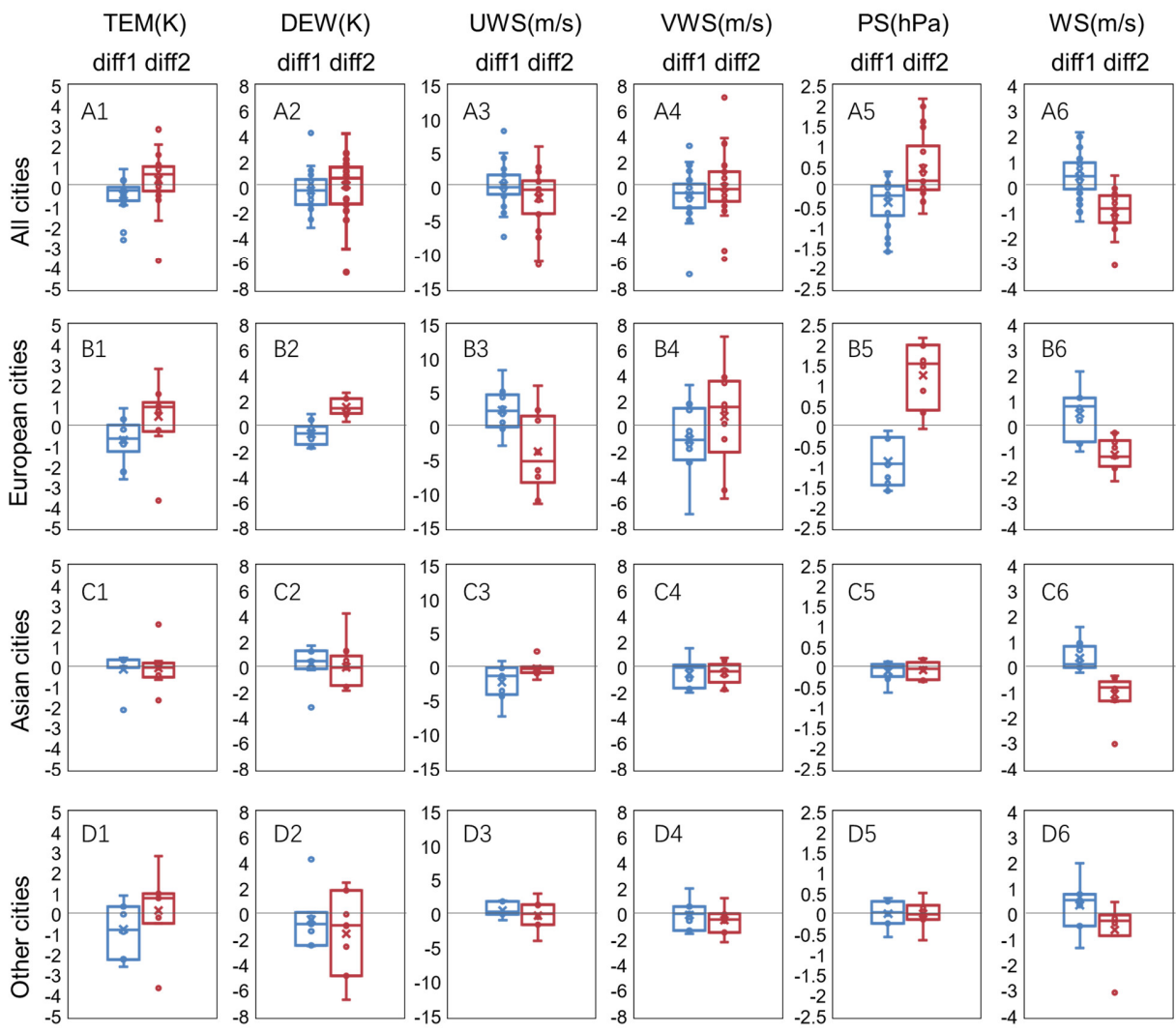
232 For a quantitative description of how much the air quality had changed under the impact of  
233 the FCCs and lockdowns, the change percent of the AQI during the different periods were  
234 calculated and summarized for several typical regions (Table S3). The results showed that both the  
235 FCCs and lockdowns brought a large reduction in NO<sub>2</sub> in most cities, with lockdowns typically  
236 bringing larger changes (22% [95% confidence interval:14%, 30%]) than the FCCs (9% [3%, 16%]).  
237 However, in Europe, the changes in NO<sub>2</sub> caused by the FCCs and lockdowns were similar (16%  
238 [7%, 26%] for the FCC and 16% [5%, 26%] for the lockdowns). An exception occurred in Patna,  
239 India, where the AQI anomalies of NO<sub>2</sub> increased greatly after the FCC (180%) and the lockdown

240 (46%). Patna was a heavily-polluted<sup>40,41</sup> and lightly-infected city. Transportation data showed that  
 241 mobility in Patna did not decrease during the COVID-19 outbreak (Figure 5A), while in Mumbai,  
 242 India, mobility decreased significantly (Figure 5B). In addition, O<sub>3</sub> in Patna decreased 103.96%  
 243 since the FCC (Figure 3, Table S1), which was the largest among all of the 26 cities. Previous  
 244 studies had shown that an inverse relationship existed between O<sub>3</sub> and NO<sub>2</sub><sup>42-44</sup>, which was also  
 245 detected by the analysis results of this study, as shown in Figure S10 (the variation trends of O<sub>3</sub> and  
 246 NO<sub>2</sub> were nearly opposite). Based on the above points, it was inferred that the ongoing human  
 247 activities and the interactions between air pollutants caused the increase in NO<sub>2</sub> in Patna.



248 **Figure 5.** Daily variations in mobility and travel intensity in four typical cities. (A, B) The mobility  
 249 variations in Patna and Mumbai, India. (C) The travel intensity variations in Wuhan and Xining,  
 250 China.  
 251

252 Additionally,  $PM_x$  also decreased by a large amount after the FCCs and lockdowns.  
253 Specifically, the lockdowns caused a decline of 24% (10%, 39%) in Asian and Africa and 12% (4%,  
254 16%) in the cities of North America, South America, and Australia. In contrast, the FCCs brought  
255 little changes to  $PM_x$  in these regions. An interesting phenomenon appeared in cities in Europe  
256 (Rome and Milan in Italy, Paris, and Nantes in France, Hamburg in Germany, and London in the  
257 U.K.).  $PM_x$  declined by 20% (14%, 32%) after the FCC, but increased greatly (28% [3%, 53%])  
258 during the European lockdowns. The meteorological data showed that European cities experienced  
259 extremely unfavorable meteorological conditions during the lockdowns (Figures S12–S13). To be  
260 specific, compared with other cities, the European cities witnessed large increases in pressure and  
261 dewpoint temperatures and a decrease in wind speeds since the lockdowns began (Figure 6). It can  
262 be inferred that the high-humidity, high-pressure, and low-wind-speed conditions offset the  
263 improvements in the  $PM_x$  pollution caused by the COVID-19 lockdowns. Asian cities and other  
264 cities have also experienced small declines in wind speed, but generally, the overall meteorological  
265 conditions did not change significantly compared with the period prior to the lockdowns.



266

267 **Figure 6.** The boxplot for the changes in the meteorological anomalies after the FCC/lockdowns  
 268 (diff1/diff2) in the different groups of cities. The blue box plots represent diff1, and the red  
 269 represent diff2. The first five meteorological factors have the same meaning as in Figure 2. The last  
 270 variable, WS, represents the composite wind speed, which was calculated from the UWS and VWS.

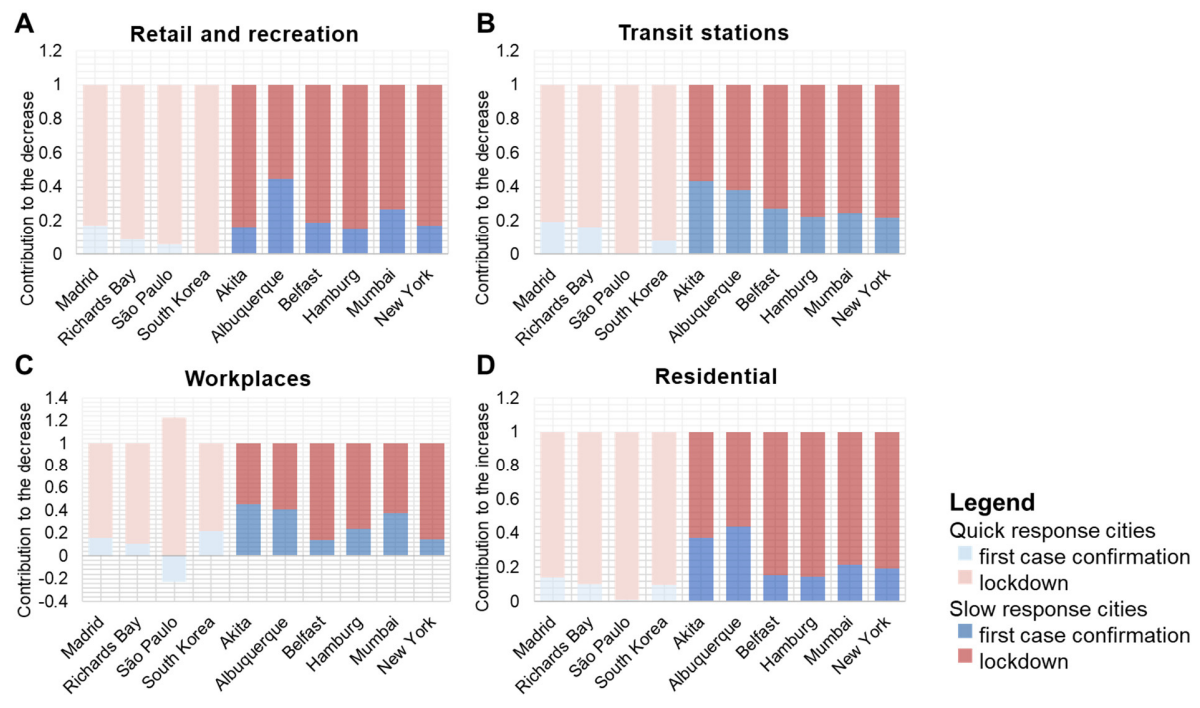
271 The changes in the other three atmospheric pollutants were not as obvious as for NO<sub>2</sub> and PM<sub>x</sub>.  
 272 Among them, O<sub>3</sub> showed an increase in some cities after the FCCs and lockdowns, which has been  
 273 paid special attention by some researchers<sup>39,45</sup>. It was inferred to be a result of a nonlinear  
 274 production chemistry of ozone in the atmosphere, and reduced nitrogen oxides resulted in ozone  
 275 enhancement<sup>39</sup>. CO showed a mild increase after the FCCs and a mild decrease during lockdown  
 276 in most regions. As for SO<sub>2</sub>, the variation trend showed strong spatial heterogeneity.

277 The impact of the FCCs and lockdowns on air quality varied with cities. In the quick-response  
278 cities (the upper portion of Figure 3), the lockdowns typically caused a larger decline than the FCCs,  
279 but in the slow-response cities (the lower portion of Figure 3), the case was more complicated, and  
280 it was likely that the effect of the FCCs and lockdowns were comparable. As mentioned earlier, in  
281 some of the slow-response cities (not all), people may have already tried to avoid going out since  
282 the appearance of the first case. The changes in human activities caused by the COVID-19  
283 pandemic happened gradually in a relatively long period of time, rather than changing sharply in a  
284 short time like in the quick-response cities. Therefore, the changes in air quality were not dominated  
285 by the lockdown, but they could have been affected by multiple factors, such as the FCCs and  
286 meteorological factors. An interesting phenomenon that can be seen in Figure 3 also demonstrates  
287 this opinion. It has been discussed that an increase in  $PM_{2.5}$  and  $PM_{10}$  after the lockdowns in  
288 European cities was caused by unfavorable meteorological conditions that offset the impact of the  
289 lockdowns. Then it was found that the offset effect was more obvious in the slow-response cities  
290 than in the quick-response cities. This is because the lockdowns had a larger impact on air quality  
291 in the quick-response cities than in the slow-response cities, which is consistent with the conclusion  
292 above.

### 293 **Mobility variation during COVID-19**

294 Finally, for a further demonstration of the above conclusions, the mobility data for different  
295 regions were utilized (Figure S11), and the contributions of the FCCs and lockdowns to the changes  
296 in mobility were calculated. The results showed similar conclusions. First, a decrease in mobility  
297 in retail and recreation places, transit stations, and workplaces was observed. Additionally, the  
298 mobility in residential areas increased during the COVID-19 outbreak (Figure S11). This result  
299 indicated a decrease in the travel frequency, which may explain the reduction in  $PM_{2.5}$ ,  $PM_{10}$ , and  
300  $NO_2$  pollution. Second, in the quick-response cities, the lockdowns contributed most to the mobility  
301 changes; however, in slow-response cities, the contribution of the FCCs to mobility change

302 increased compared with the quick-response cities (Figure 7). This may explain why the lockdowns  
 303 had a larger impact on air quality in the quick-response cities than in the slow-response cities. The  
 304 consistency between the mobility changes and air quality changes also revealed the relationship  
 305 between human activities and atmospheric pollution.



306 **Figure 7.** The contribution of the FCCs/lockdowns to the total mobility declines (increase for (D))  
 307 in different places. The cities represented by the light color bars are the quick-response cities, and  
 308 the others are the slow-response cities. The red portions are the contributions of the lockdowns and  
 309 the blue is the contribution of the FCCs.

311 **Discussion**

312 **Difference in trends between the original observations and the anomalies**

313 Most air pollutants can vary with months under the impact of meteorological conditions (for  
 314 example PM<sub>2.5</sub> may decrease from January to April, and O<sub>3</sub> may increase from January to April in  
 315 China)<sup>46,47</sup>. Therefore, the pollutant anomalies concentration data for 2020 were calculated using  
 316 data from previous years as a baseline to remove the impact of the inner pollutant variation trends.  
 317 The MK test results are shown in Figure 1. For comparison, the MK test was also conducted on the

318 original pollutant observations for the same time period (Figure S14). As shown, there is a clear  
319 difference between the original observations and the anomalies.

320  $PM_x$  increased in most areas with high latitudes in the northern hemisphere, but the  $PM_x$   
321 anomalies showed an opposite trend in northern China, the northern U.S., and areas near the Arctic  
322 Circle. However, in western Australia,  $PM_x$  showed a significant downtrend in the original results,  
323 but not a significant downtrend or even an uptrend in the anomaly results. Although two kinds of  
324 results for  $NO_2$  showed similar variation trends in most areas of the world, except for northern  
325 Southeast Asia and western China, the significances of the anomalies were lower than those of the  
326 original observations on the whole. The spatial distribution of the original  $O_3$  observations had  
327 obvious characteristics of latitude stratification. The temperature and solar radiation in areas near  
328 the equator are higher and stronger, and this is favorable for the production of  $O_3$ <sup>48</sup>. A similar but  
329 less obvious pattern was observed in the  $O_3$  anomaly results. The original  $SO_2$  results showed a  
330 more significant uptrend near the equator as well. As for CO, the original observations increased  
331 significantly in most areas of the northern hemisphere. The northern hemisphere is subject to dry  
332 weather conditions from September to March of the following year, and this is the peak season for  
333 hill fires in the northern hemisphere, which will lead to rapid increases in CO concentrations<sup>49</sup>.  
334 However, the anomaly results displayed a totally different pattern. In most areas, CO had no  
335 significant variation, which meant that the change in CO was caused by its inner periodicity affected  
336 by meteorological conditions. As demonstrated above, the process of calculating anomalies  
337 effectively eliminated the inner variation pollution trends and improved the accuracy of this  
338 analysis.

### 339 **Impact of work resumption**

340 During the study period, two cities, namely, Wuhan and Xining, had ended their lockdown  
341 and started to resume work and production, which is usually accompanied by a resumption of  
342 human activities. Therefore, it will be interesting to observe the air quality changes after work

343 resumption. Wuhan gradually began to resume work and production in week 12. The satellite and  
344 reanalysis data showed that the NO<sub>2</sub> anomalies in the Wuhan area started to show an increasing  
345 trend after week 12. During week 13, the anomalies turned to large positive values, indicating a  
346 large increase compared with the NO<sub>2</sub> concentrations of previous years. The ground-based  
347 measurements showed similar results. Specifically, in Wuhan, the PM<sub>2.5</sub>, PM<sub>10</sub>, and NO<sub>2</sub> increased  
348 by 12.85%, 15.29%, and 38.08%, respectively, after work resumption. In Xining, the work  
349 resumption led to an increase of 16.68%, 73.25%, and 7.01%, for PM<sub>2.5</sub>, PM<sub>10</sub>, and NO<sub>2</sub>,  
350 respectively. Apart from PM<sub>x</sub> and NO<sub>2</sub>, SO<sub>2</sub> also showed an increase (39.37% for Wuhan and 11.57%  
351 for Xining), while the changes in CO and O<sub>3</sub> were mild.

352 The variations in transportation data in Wuhan and Xining were also analyzed (Figure 5C).  
353 The results showed that the travel intensity began to increase after February 17, 2020, when Xining  
354 started to resume work and production. In Wuhan, the case was similar, and travel intensity began  
355 to increase after March 25, 2020. The change in air quality could be closely related to the changes  
356 in transportation, which again, revealed the relationship between air pollution and human activities.

## 357 **Conclusion**

358 Industrial development has been accused of being the primary cause of air pollution in the past  
359 several decades. The breakout of the COVID-19 pandemic has provided a special test foundation  
360 to investigate the relationship between them. In this study, multisource data were utilized to  
361 quantify the air quality changes and the impacts of COVID-19 FCCs and lockdowns on air quality  
362 changes. The results showed that the COVID-19-related human activity slowdowns resulted in the  
363 greatest reduction in NO<sub>2</sub> pollution, which dropped by approximately 30% since the COVID-19  
364 breakout on the global scale. Then the PM<sub>2.5</sub> and PM<sub>10</sub>. Most cities witnessed a percentage decline  
365 of approximately 20%, except for cities in Europe. Unfavorable meteorological conditions since  
366 the end of March in European cities offset the influence of the lockdowns, and this worsened PM<sub>2.5</sub>  
367 and PM<sub>10</sub> pollution. The changes in O<sub>3</sub>, SO<sub>2</sub>, and CO pollution were not as obvious as for PM<sub>x</sub> and

368 NO<sub>2</sub>, but indications of ozone enhancement and CO decreases were seen in some areas. While most  
369 current studies have focused only on the impact of lockdowns and have concluded that lockdowns  
370 are followed by air quality improvements, this study found that this was not always the case. In  
371 those cities with a relatively quick responses to the outbreak of the COVID-19 pandemic, the effect  
372 of lockdowns on air quality was typically significant, but for the slow-response cities, the effect of  
373 FCCs and meteorological parameters on air quality was found to also be significant.

374 Although this study has drawn numerous valuable conclusions, there are still limitations of  
375 this study. For example, the observations from TROPOMI only provided information on the  
376 total/tropospheric vertical column for the different atmospheric pollutants, which may not be  
377 greatly affected by human activities/emission sources in some regions. As a consequence, future  
378 work must first aim at generating high-accuracy global ground-level concentrations of each  
379 atmospheric pollutant by combing multiple datasets (e.g., ground-based sites and TROPOMI). Next,  
380 the generated results were employed for the analyses of air quality, which is expected to indicate  
381 more significant temporal variations related to the human activities/emission sources. Additionally,  
382 the results of this study were primarily obtained from the statistical analysis, which may be  
383 insufficient for exploring the reasons for air quality changes. Although a detailed and  
384 comprehensive investigation was conducted regarding the air quality changes during COVID-19,  
385 there are some results that were not fully explained. It is hoped that these findings can provide some  
386 interesting topics or directions for atmospheric chemistry or model simulation researchers, and  
387 taken together, our understanding of COVID-19's impact on the atmosphere can be further  
388 improved. Finally, as some studies have proposed<sup>33,53</sup>, COVID-19 has not only had a short-run  
389 influence on the earth system, but it can also have a long-run impact. Long-term and continuous  
390 observations and analyses will be of great significance in the future.

391 **Resource availability**

392 **Data and code availability**

393 Satellite products were download from <https://disc.gsfc.nasa.gov/>. Reanalysis products are  
394 accessible at <https://apps.ecmwf.int/datasets/data/cams-nrealtime/levtype=sfc/>. Global air quality  
395 index data are accessible at <https://aqicn.org/>. Transportation data of China was supported by the  
396 Baidu migration dataset (<https://qianxi.baidu.com>), while those of other countries were provided  
397 by Google mobility reports (<https://www.google.com/covid19/mobility/>). For more details  
398 regarding the datasets and preprocessing, please refer to the supplemental experimental procedures  
399 section. The methods described in this article were implemented using MATLAB (R2020a). The  
400 specific datasets and codes used in this study are available from the lead contact on request.

## 401 **Materials and methods**

### 402 **Time series analysis for the satellite and reanalysis data.**

403 First, the pollutant anomalies were calculated using previous observations as a baseline to  
404 remove the impact of the inner pollutant variation trends, which has been a widely used and  
405 effective strategy found in similar studies<sup>18,39,50-52</sup>.

$$406 \quad abCon_j = Con_{j,2020} - \sum_{i=2017}^{2019} Con_{j,i} / 3, \quad (1)$$

407 where *Con* means the concentration data; *j* represents the types of air pollutants, including PM<sub>2.5</sub>,  
408 PM<sub>10</sub>, SO<sub>2</sub>, NO<sub>2</sub>, O<sub>3</sub>, and CO; and *i* represents the previous years, from 2017 to 2019. Negative  
409 anomalies show that the air pollution decreased in 2020 compared with the previous three years,  
410 and vice versa. Specifically, for the SO<sub>2</sub> and CO data, and only data from 2019 were used to  
411 calculate the anomalies due to the lack of data for 2017 and 2018.

412 The MK test was then conducted on the anomalies of six pollutants from January 1 to March  
413 31, 2020 to show the trends. Additionally, to reduce the interference of small fluctuations on the  
414 results, an average of the anomalies was taken every three days prior to the MK test.

### 415 **Time series analysis for the ground-based data**

416 Similar to the satellite and reanalysis data, first the anomalies of the ground-based AQI data  
417 were calculated using the following formula:

418 
$$abAQI_j = AQI_{j,2020} - \sum_{i=2017}^{2019} AQI_{j,i} / 3 \quad . \quad (2)$$

419 Specially, for the AQI data in Tehran, Iran, data from 2017 were lacking, and only data for  
 420 2018 and 2019 were used as the baseline. For the PM<sub>2.5</sub>, NO<sub>2</sub>, and O<sub>3</sub> AQIs in Richards Bay, South  
 421 Africa, data for 2017 and 2018 were lacking, and only data from 2019 were used as the baseline.

422 For the ground station data, two junctures were researched: time of the first confirmed case  
 423 ( $t_{fc}$ ), time of lockdown ( $t_{lk}$ ), and one juncture was considered: the time of reopen ( $t_{op}$ ). Two steps  
 424 were then used to conduct the analysis.

425 Step one, two quantitative indicators were designed to describe the changes in air quality after  
 426 the beginning of COVID-19 (time of first case confirmation in the country) and the lockdowns.

427 
$$diff_{1,j} = \sum_{t=t_{fc}}^{t_{lk}-1} abAQI_{j,t} / (t_{lk} - t_{fc}) - \sum_{t=t_0}^{t_{fc}-1} abAQI_{j,t} / (t_{fc} - t_0) \quad , \quad (3)$$

428 
$$diff_{2,j} = \sum_{t=t_{lk}}^{t_{op}-1} abAQI_{j,t} / (t_{op} - t_{lk}) - \sum_{t=t_{fc}}^{t_{lk}-1} abAQI_{j,t} / (t_{lk} - t_{fc}) \quad , \quad (4)$$

429 where  $j$  represents the types of air pollutants;  $diff_1$  and  $diff_2$  stand for the changes in the AQI after  
 430 the first confirmed case and during lockdown, respectively;  $t_0$  represents the first day of the total  
 431 research period, i.e., January 1, 2020;  $t_{fc}$ ,  $t_{lk}$ , and  $t_{op}$  represent the time for first confirmed case in  
 432 the country, lockdown, and reopen. Then, using the average AQI value during period 1 (from  $t_0$  to  
 433  $t_{fc}$ ) and period 2 (from  $t_{fc}$  to  $t_{lk}$ ) in 2020 as a baseline, the percent of change was calculated:

434 
$$per_{1,j} = \frac{diff_{1,j}}{\sum_{t=t_0}^{t_{fc}-1} AQI_{j,t} / (t_{fc} - t_0)} \times 100\% \quad , \quad (5)$$

435 
$$per_{2,j} = \frac{diff_{2,j}}{\sum_{t=t_{fc}}^{t_{lk}-1} AQI_{j,t} / (t_{lk} - t_{fc})} \times 100\% \quad . \quad (6)$$

436 In step two, a max-mean-value method was used to detect the point where the tendency of  
 437 time series began to change. To avoid the impact of some extreme values and concentrate on the  
 438 overall trend, a 15-day moving average for the abnormal AQI time series ( $sAQI$ ) was used. Then,

439 every time point in the smoothed time series was searched, and the one that had the largest  
 440 difference the times series before and after the time point in the mean values was located. This  
 441 process can be expressed as:

$$442 \quad t_j^* = \arg \max_{t_j^*} \left| \sum_{t=t_0}^{t_j^*-1} sAQI_{j,t} / (t_j^* - t_0) - \sum_{t=t_j^*}^{t_{op}} sAQI_{j,t} / (t_{op} - t_j^* + 1) \right| , \quad (7)$$

443 where  $j$  represents the types of air pollutants;  $sAQI$  represents the smoothed abnormal AQI time  
 444 series after a 15-day moving average;  $t^*$  stands for the detected time point and is referred to as the  
 445 ‘change point’ in the main text;  $t_0$  represents the first day of the total research period, i.e., January  
 446 1, 2020; and  $t_{op}$  represents the time of reopening (lockdown end). The Pearson correlation  
 447 coefficients between the change point, FCC, and lockdown times were then calculated.

#### 448 **Transportation change analysis**

449 The change in accessible mobility during the entire study period (February 15 to April 24,  
 450 2020) was divided into two parts: change after the first case confirmation and change after the  
 451 lockdown began. The contribution of each part to the total decline in mobility was calculated using  
 452 the following formula:

$$453 \quad dTrans_1 = diff_{1,Trans} / (diff_{1,Trans} + diff_{2,Trans}) , \quad (8)$$

$$454 \quad dTrans_2 = diff_{2,Trans} / (diff_{1,Trans} + diff_{2,Trans}) , \quad (9)$$

455 where  $dTrans_1$  and  $dTrans_2$  represent the contribution of the first case confirmation and the  
 456 lockdown to the total decline in mobility, respectively. In addition,

$$457 \quad diff_{1,Trans} = \sum_{t=t_{fc}}^{t_{lk}-1} Trans_t / (t_{lk} - t_{fc}) - \sum_{t=t_0}^{t_{fc}-1} Trans_t / (t_{fc} - t_0) , \quad (10)$$

$$458 \quad diff_{2,Trans} = \sum_{t=t_{lk}}^{t_{op}-1} Trans_t / (t_{op} - t_{lk}) - \sum_{t=t_{fc}}^{t_{lk}-1} Trans_{j,t} / (t_{lk} - t_{fc}) , \quad (11)$$

459 where  $Trans_t$  represents the mobility at day  $t$ .

#### 460 **Meteorological change analysis**

461 The analysis of meteorological condition changes during this time period was similar to that of  
 462 the ground-based AQI data, which included two primary steps. First, the anomalies of 2020 were  
 463 calculated using the average value of 2017–2019 as the baseline. Then the variations in the daily  
 464 anomalies in 2020 were divided into two parts: change after the first case confirmation and change  
 465 after the lockdown started, which are calculated in the same way as the AQI change and  
 466 transportation change. The composite wind speed (WS) was calculated from the zonal wind (UWS)  
 467 and meridional wind (VWS) using the following formula:

$$468 \quad WS = \sqrt{UWS^2 + VWS^2} . \quad (12)$$

### 469 The Mann-Kendall (MK) test

470 As a non-parametric statistical test method, MK does not require samples to follow a certain  
 471 distribution and not be disturbed by a few outliers<sup>54</sup>. It is often applied to trend analyses and  
 472 mutation detections in time series. Assuming that  $X_1, X_2, \dots, X_n$  is a set of time-series data, the test  
 473 statistic,  $S$ , is defined by the following equations:

$$474 \quad S = \sum_{i=2}^n \sum_{j=1}^{i-1} \text{sign}(X_i - X_j), \quad (13)$$

$$475 \quad \text{sign}(X_i - X_j) = \begin{cases} 1, (X_i - X_j) > 0 \\ 0, (X_i - X_j) = 0 \\ -1, (X_i - X_j) < 0 \end{cases} , \quad (14)$$

$$476 \quad \text{vars}(S) = n(n-1)(2n+5)/18 , \quad (15)$$

477 where  $S$  is normally distributed with a mean of 0; and  $\text{vars}(S)$  is the variance of  $S$ .

478 Then the  $Z$  statistic is calculated to indicate variation trends of the time series data if  $n$  was  
 479 greater than 10:

$$480 \quad Z = \begin{cases} \frac{S-1}{\sqrt{\text{var}(S)}}, S > 0 \\ 0, S = 0 \\ \frac{S+1}{\sqrt{\text{var}(S)}}, S < 0 \end{cases} . \quad (16)$$

481 The variation trend of a time series manifests as an increasing tendency when  $Z$  is positive,  
482 while a negative  $Z$  indicates a decreasing tendency. Additionally, the variation trend is significant  
483 (95% significance level) when the absolute value of  $Z$  exceeds 1.64 and is extremely significant  
484 (95% significance level) when the absolute value of  $Z$  exceeds 2.32.

## 485 **Acknowledgments**

486 We thank all of the individuals and organizations who collected air quality data and other  
487 relevant data during the COVID-19 outbreak around the world. We gratefully acknowledge the  
488 support from the Strategic Priority Research Program of the Chinese Academy of Sciences (No.  
489 XDA19090104) and the National Natural Science Foundation of China (Nos. 41922008).

## 490 **Author contributions**

491 L.Z. and Qiangqiagn Yuan conceived the study. Qiangqiang Yuan, Qianqian Yang, B.W., and  
492 Y.W. developed the methods, collected the data, performed analyses, and co-wrote the manuscript,  
493 and they contributed equally to this work. T.L., C.J., J.W., S.L., and M.L. contributed to the data  
494 analysis and interpretation of the results. L.Z., H.S., and Qiangqiang Yuan reviewed and edited the  
495 manuscript.

## 496 **Declaration of interests**

497 The authors declare no competing interests.

## 498 **References**

- 499 1. Klepeis, N.E., Nelson, W.C., Ott, W.R., Robinson, J.P., Tsang, A.M., Switzer, P., Behar, J.  
500 V, Hern, S.C., And Engelmann, W.H. (2001). The National Human Activity Pattern Survey  
501 (NHAPS): a resource for assessing exposure to environmental pollutants. *J. Expo. Sci.*  
502 *Environ. Epidemiol.* 11, 231–252.

- 503 2. Ezzati, M., Lopez, A. D., Rodgers, A. A., Murray, C. J. (2004). Comparative quantification  
504 of health risks: global and regional burden of disease attributable to selected major risk  
505 factors. World Health Organization.
- 506 3. Brunekreef, B., and Holgate, S.T. (2002). Air pollution and health. *Lancet* 360, 1233–1242.
- 507 4. Cohen, A.J., Brauer, M., Burnett, R., Anderson, H.R., Frostad, J., Estep, K., Balakrishnan, K.,  
508 Brunekreef, B., Dandona, L., Dandona, R., et al. (2017). Estimates and 25-year trends of the  
509 global burden of disease attributable to ambient air pollution: an analysis of data from the  
510 Global Burden of Diseases Study 2015. *Lancet* 389, 1907–1918.
- 511 5. Ambient air pollution, World Health Organization.  
512 <https://www.who.int/airpollution/ambient/health-impacts/en/> [accessed 9 October 2020]
- 513 6. Akimoto, H. (2003). Global Air Quality and Pollution. *Science* 302(5651), 1716–1719.
- 514 7. Team, T.N.C.P.E.R.E. The Epidemiological Characteristics of an Outbreak of 2019 Novel  
515 Coronavirus Diseases (COVID-19) — China, 2020. *China CDC Wkly.* 2, 113–122.
- 516 8. Zhu, N., Zhang, D., Wang, W., Li, X., Yang, B., Song, J., Zhao, X., Huang, B., Shi, W., Lu,  
517 R., et al. (2020). A Novel Coronavirus from Patients with Pneumonia in China, 2019. *N.*  
518 *Engl. J. Med.* 382, 727–733.
- 519 9. Guan, W., Ni, Z., Hu, Y., Liang, W., Ou, C., He, J., Liu, L., Shan, H., Lei, C., Hui, D.S.C., et  
520 al. (2020). Clinical Characteristics of Coronavirus Disease 2019 in China. *N. Engl. J. Med.*  
521 382, 1708–1720.
- 522 10. Remuzzi, A., and Remuzzi, G. (2020). COVID-19 and Italy: what next? *Lancet* 395, 1225–  
523 1228.

- 524 11. Mizumoto, K., Kagaya, K., Zarebski, A., and Chowell, G. (2020). Estimating the  
525 asymptomatic proportion of coronavirus disease 2019 (COVID-19) cases on board the  
526 Diamond Princess cruise ship, Yokohama, Japan, 2020. *Eurosurveillance* 25.
- 527 12. COVID, CDC, and Response Team. (2020). Severe outcomes among patients with  
528 coronavirus disease 2019 (COVID-19)—United States, February 12–March 16, 2020.  
529 *MMWR Morb Mortal Wkly Rep*, 69(12), 343-346.
- 530 13. Sohrabi, C., Alsafi, Z., O’Neill, N., Khan, M., Kerwan, A., Al-Jabir, A., Iosifidis, C., and  
531 Agha, R. (2020). World Health Organization declares global emergency: A review of the  
532 2019 novel coronavirus (COVID-19). *Int. J. Surg.* 76, 71–76.
- 533 14. Anderson, R.M., Heesterbeek, H., Klinkenberg, D., and Hollingsworth, T.D. (2020). How  
534 will country-based mitigation measures influence the course of the COVID-19 epidemic?  
535 *Lancet* 395, 931–934.
- 536 15. World Health Organization. (2020). Assessment of risk factors for coronavirus disease 2019  
537 (COVID-19) in health workers: protocol for a case-control study, 26 May 2020 (No.  
538 WHO/2019-nCoV/HCW\_RF\_CaseControlProtocol/2020.1). World Health Organization.
- 539 16. Wu, Z., and McGoogan, J.M. (2020). Characteristics of and Important Lessons from the  
540 Coronavirus Disease 2019 (COVID-19) Outbreak in China: Summary of a Report of 72 314  
541 Cases From the Chinese Center for Disease Control and Prevention. *JAMA* 323, 1239–1242.
- 542 17. World Health Organization, Coronavirus disease (COVID-2019) situation reports;  
543 <https://www.who.int/emergencies/diseases/novel-coronavirus-2019/situation-reports/>  
544 [accessed 9 October 2020]
- 545 18. Tian, H., Liu, Y., Li, Y., Wu, C.-H., Chen, B., Kraemer, M.U.G., Li, B., Cai, J., Xu, B.,  
546 Yang, Q., et al. (2020). An investigation of transmission control measures during the first 50  
547 days of the COVID-19 epidemic in China. *Science*. 368, 638 – 642.

- 548 19. Chinazzi, M., Davis, J.T., Ajelli, M., Gioannini, C., Litvinova, M., Merler, S., Pastore y  
549 Piontti, A., Mu, K., Rossi, L., Sun, K., et al. (2020). The effect of travel restrictions on the  
550 spread of the 2019 novel coronavirus (COVID-19) outbreak. *Science*. 368, 395– 400.
- 551 20. Saraswat, R., and Saraswat, D.A. (2020). Research opportunities in pandemic lockdown.  
552 *Science*. 368, 594 – 595.
- 553 21. Rosenbloom, D., and Markard, J. (2020). A COVID-19 recovery for climate. *Science*. 368,  
554 447 – 447.
- 555 22. He, G., Pan, Y., and Tanaka, T. (2020). The short-term impacts of COVID-19 lockdown on  
556 urban air pollution in China. *Nat. Sustain.* <https://doi.org/10.1038/s41893-020-0581-y>
- 557 23. Mahato, S., Pal, S., and Ghosh, K.G. (2020). Effect of lockdown amid COVID-19 pandemic  
558 on air quality of the megacity Delhi, India. *Sci. Total Environ.* 730, 139086.
- 559 24. Wang, Q., and Su, M. (2020). A preliminary assessment of the impact of COVID-19 on  
560 environment – A case study of China. *Sci. Total Environ.* 728, 138915.
- 561 25. Sharma, S., Zhang, M., Anshika, Gao, J., Zhang, H., and Kota, S.H. (2020). Effect of  
562 restricted emissions during COVID-19 on air quality in India. *Sci. Total Environ.* 728,  
563 138878.
- 564 26. Huang, X., Ding, A., Gao, J., Zheng, B., Zhou, D., Qi, X., Tang, R., Wang, J., Ren, C., Nie,  
565 W. (2020). Enhanced secondary pollution offset reduction of primary emissions during  
566 COVID-19 lockdown in China. *National Science Review*.
- 567 27. Shi, X., Brasseur., G.P. (2020). The response in air quality to the reduction of Chinese  
568 economic activities during the COVID-19 outbreak, *Geophys. Res. Lett.*, 47 (11),  
569 e2020GL088070.

- 570 28. Bauwens, M., Compernelle, S., Stavrakou, T., Müller, J.-F., van Gent, J., Eskes, H., Levelt,  
571 P.F., van der A, R., Veefkind, J.P., Vlietinck, J., et al. (2020). Impact of Coronavirus  
572 Outbreak on NO<sub>2</sub> Pollution Assessed Using TROPOMI and OMI Observations. *Geophys.*  
573 *Res. Lett.* 47, e2020GL087978.
- 574 29. Chen, H., Huo, J., Fu, Q., Duan, Y., Xiao, H., Chen, J. (2020). Impact of quarantine measures  
575 on chemical compositions of PM<sub>2.5</sub> during the COVID-19 epidemic in Shanghai, China. *Sci.*  
576 *Total Environ.*, 743, 140758.
- 577 30. Rodríguez-Urrego, D., Rodríguez-Urrego, L. (2020). Air quality during the COVID-19:  
578 PM<sub>2.5</sub> analysis in the 50 most polluted capital cities in the world. *Environ. Pollut.*, 115042.
- 579 31. Chu, B., Zhang, S., Liu, J., Ma, Q., He, H. (2020). Significant concurrent decrease in PM<sub>2.5</sub>  
580 and NO<sub>2</sub> concentrations in China during COVID-19 epidemic. *Journal of Environ. Sci.*, 99,  
581 346-353.
- 582 32. Venter, Z. S., Aunan, K., Chowdhury, S., Lelieveld, J. (2020). COVID-19 lockdowns cause  
583 global air pollution declines. *P. Natl. Acad. Sci. USA.*, 117(32), 18984-18990.
- 584 33. Diffenbaugh, N. S., Field, C. B., Appel, E. A., Azevedo, I. L., Baldocchi, D. D., Burke, M.,  
585 Burney, J. A., Ciais, P., Davis, S. J., Fiore, A. M. et al. (2020). The COVID-19 lockdowns: a  
586 window into the Earth System, *Nature Reviews Earth Environment*, 1, 470–481.
- 587 34. Zhang, Z., Arshad, A., Zhang, C., Hussain, S., Li, W. (2020). Unprecedented temporary  
588 reduction in global air pollution associated with COVID-19 forced confinement: A  
589 continental and city scale analysis. *Remote Sens.*, 12(15), 2420.
- 590 35. Guan, Q., Yang, Y., Luo, H., Zhao, R., Pan, N., Lin, J., Yang, L. (2019). Transport pathways  
591 of PM<sub>10</sub> during the spring in northwest China and its characteristics of potential dust sources.  
592 *J. Cleaner Prod.* 237(10), 117746.

- 593 36. Hashem, T. M., Zirlewagen, M., & Braun, A. M. (1997). Simultaneous photochemical  
594 generation of ozone in the gas phase and photolysis of aqueous reaction systems using one  
595 VUV light source. *Water Science and Technology*, 35(4), 41-48.
- 596 37. Saglietto, A., D'Ascenzo, F., Zoccai, G.B., and De Ferrari, G.M. (2020). COVID-19 in  
597 Europe: the Italian lesson. *Lancet* 395, 1110–1111.
- 598 38. Kupferschmidt, K., and Cohen, J. (2020). Can China's COVID-19 strategy work elsewhere?  
599 *Science*. 367, 1061–1062.
- 600 39. Le, T., Wang, Y., Liu, L., Yang, J., Yung, Y. L., Li, G., Seinfeld, J. H. (2020). Unexpected  
601 air pollution with marked emission reductions during the COVID-19 outbreak in China.  
602 *Science*, 369(6504), 702-706.
- 603 40. Kota, S.H., Guo, H., Myllyvirta, L., Hu, J., Sahu, S.K., Garaga, R., Ying, Q., Gao, A.,  
604 Dahiya, S., Wang, Y., et al. (2018). Year-long simulation of gaseous and particulate air  
605 pollutants in India. *Atmos. Environ.* 180, 244–255.
- 606 41. Arif, M., Kumar, R., Kumar, R., Eric, Z., and Gourav, P. (2018). Ambient black carbon,  
607 PM<sub>2.5</sub> and PM<sub>10</sub> at Patna: Influence of anthropogenic emissions and brick kilns. *Sci. Total*  
608 *Environ.* 624, 1387–1400.
- 609 42. Ripperton, L. A., Kornreich, L., Worth, J. J. (1970). Nitrogen dioxide and nitric oxide in non-  
610 urban air. *Journal of the Air Pollution Control Association*, 20(9), 589-592.
- 611 43. Han, S., Bian, H., Feng, Y., Liu, A., Li, X., Zeng, F., Zhang, X. (2011). Analysis of the  
612 Relationship between O<sub>3</sub>, NO and NO<sub>2</sub> in Tianjin, China. *Aerosol and Air Quality Research*,  
613 11(2), 128-139.
- 614 44. Wang, T., Cheung, V.T.F., Anson, M., Li, Y.S. (2001). Ozone and related gaseous pollutants  
615 in the boundary layer of eastern China: Overview of the recent measurements at a rural site.  
616 *Geophys. Res. Lett.* 28, 2373–2376.

- 617 45. Hashim, B. M., Al-Naseri, S. K., Al-Maliki, A., Al-Ansari, N. (2020). Impact of COVID-19  
618 lockdown on NO<sub>2</sub>, O<sub>3</sub>, PM<sub>2.5</sub> and PM<sub>10</sub> concentrations and assessing air quality changes in  
619 Baghdad, Iraq. *Sci. Total Environ.*, 141978.
- 620 46. Melkonyan, A., and Kuttler, W. (2012). Long-term analysis of NO, NO<sub>2</sub> and O<sub>3</sub>  
621 concentrations in North Rhine-Westphalia, Germany. *Atmos. Environ.* 60, 316–326.
- 622 47. Li, T., Shen, H., Yuan, Q., Zhang, X., and Zhang, L. (2017). Estimating Ground-Level PM<sub>2.5</sub>  
623 by Fusing Satellite and Station Observations: A Geo-Intelligent Deep Learning Approach.  
624 *Geophys. Res. Lett.* 44, 11,911-985,993.
- 625 48. Wang, Z., Li, Y., Chen, T., Zhang, D., Sun, F., Wei, Q., Dong, X., Sun, R., Huan, N., and  
626 Pan, L. (2015). Ground-level ozone in urban Beijing over a 1-year period: Temporal  
627 variations and relationship to atmospheric oxidation. *Atmos. Res.* 164–165, 110–117.
- 628 49. Wotawa, G., and Trainer, M. (2000). The Influence of Canadian Forest Fires on Pollutant  
629 Concentrations in the United States. *Science.* 288, 324–328.
- 630 50. Berman, J. D., Ebisu, K. (2020). Changes in U.S. air pollution during the COVID-19  
631 pandemic. *Sci. Total Environ.* 739(15), 139864.
- 632 51. Liu, F., Page, A., Strode, S. A., Yoshida, Y., Choi, S., Zheng, B., Lamsal, L. N., Li, C.,  
633 Krotkov, N. A., Eskes, H. (2020). Abrupt decline in tropospheric nitrogen dioxide over China  
634 after the outbreak of COVID-19. *Sci. Adv.* 6(28), eabc2992.
- 635 52. Chen, K., Wang, M., Huang, C., Kinney, P. L., Anastas, P. T. (2020). Air pollution reduction  
636 and mortality benefit during the COVID-19 outbreak in China. *Lancet Planet. Health* 4(6),  
637 e210-e212.
- 638 53. Gillingham, K. T., Knittel, C. R., Li, J., Ovaere, M., & Reguant, M. (2020). The Short-run  
639 and Long-run Effects of Covid-19 on Energy and the Environment. *Joule*, 4(7), 1337-1341.
- 640 54. Yue, S., Pilon, P., and Cavadias, G. (2002). Power of the Mann–Kendall and Spearman’s rho  
641 tests for detecting monotonic trends in hydrological series. *J. Hydrol.* 259, 254–271.

642 **Supplemental files for: Global air quality change during COVID-19: a synthetic**  
643 **result of human activities and meteorology**

644 **Qianqian Yang<sup>1,\*</sup>, Bin Wang<sup>1,\*</sup>, Yuan Wang<sup>1,\*</sup>, Qiangqiang Yuan<sup>1,\*</sup>, Caiyi Jin<sup>1</sup>, Jiwen**  
645 **Wang<sup>1</sup>, Shuwen Li<sup>1</sup>, Muyu Li<sup>1</sup>, Tongwen Li<sup>2,†</sup>, Song Liu<sup>3</sup>, Huanfeng Shen<sup>2</sup>, Liangpei**  
646 **Zhang<sup>4</sup>**

647 <sup>1</sup> School of Geodesy and Geomatics, Wuhan University, Wuhan, China.

648 <sup>2</sup> School of Resource and Environmental Sciences, Wuhan University, Wuhan, China.

649 <sup>3</sup> Deutsches Zentrum für Luft- und Raumfahrt (DLR), Institut für Methodik der Fernerkundung  
650 (IMF), Oberpfaffenhofen, Germany

651 <sup>4</sup> State Key Laboratory of Information Engineering in Surveying, Mapping and Remote Sensing,  
652 Wuhan University, Wuhan, China.

653 Corresponding author: Qiangqiang Yuan ([qqyuan@sgg.whu.edu.cn](mailto:qqyuan@sgg.whu.edu.cn)).

654 \*These authors contributed equally: Qianqian Yang, Bin Wang, Yuan Wang, Qiangqiang Yuan.

655 †Present address: School of Geospatial Engineering and Science, Sun Yat-Sen University,  
656 Guangzhou, China

657  
658  
659 **Contents:**

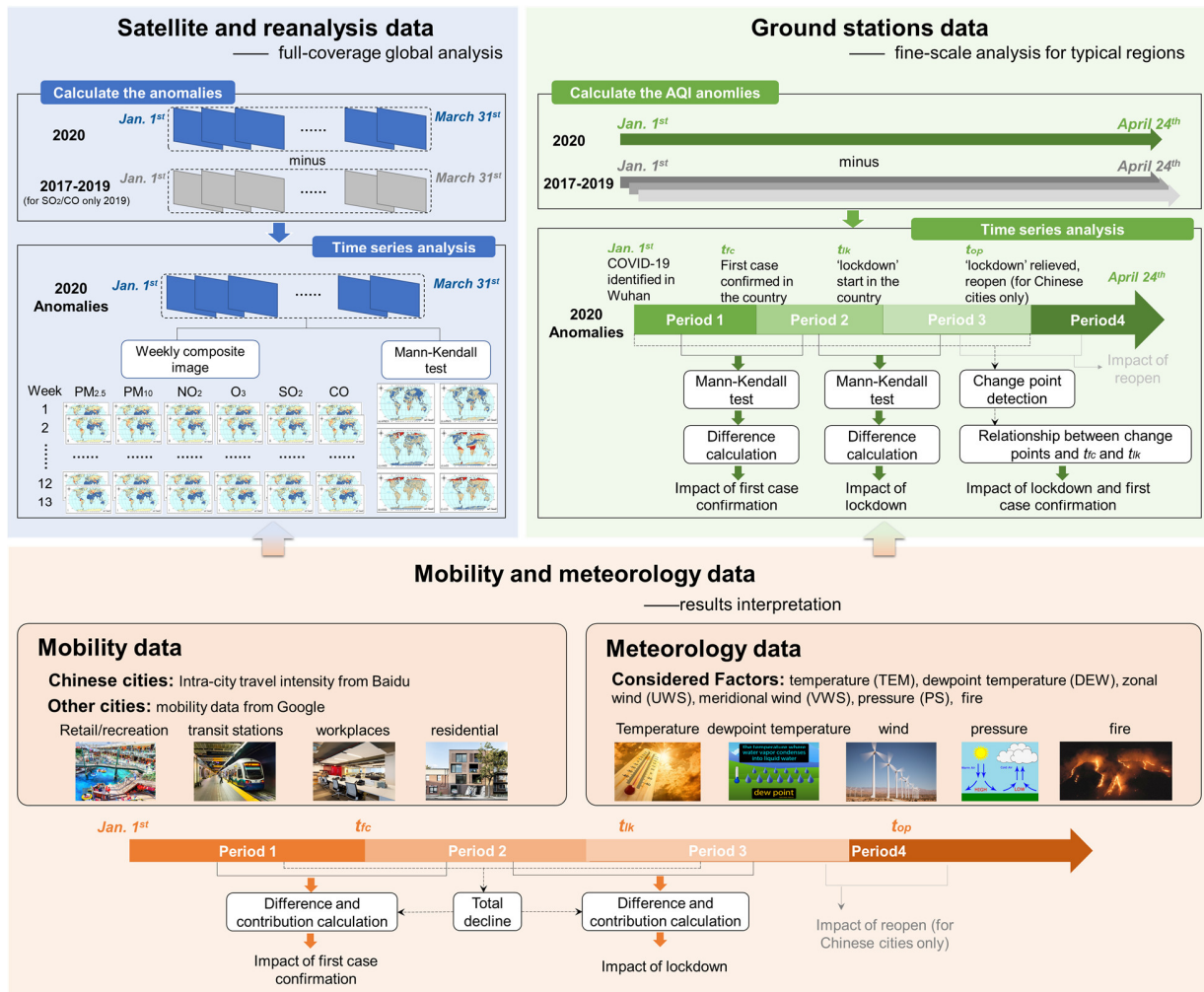
660 Supplemental Figures: Figure S1-14

661 Supplemental Tables: Table S1-4

662 Supplemental Materials and Method

663 Supplemental References  
664

# Supplemental Figures



666

667

668

669

670

671

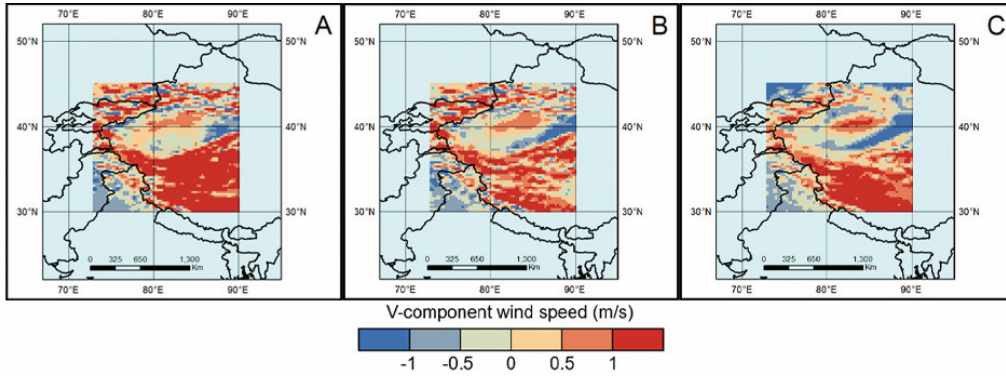
672

673

674

675

**Figure S1.** Flowchart of the work. Firstly, for a full-coverage investigation of the global air quality change were analyzed using satellite and reanalysis data via MK test. Secondly, for a fine-scale analysis of typical regions, we selected 26 typical cities around the world and analyzed the air quality index (AQI) data of six main atmospheric pollutants from local environmental monitoring stations. Finally, combined with the mobility and meteorology data, we tried to make a better explanation of the conclusions we got.



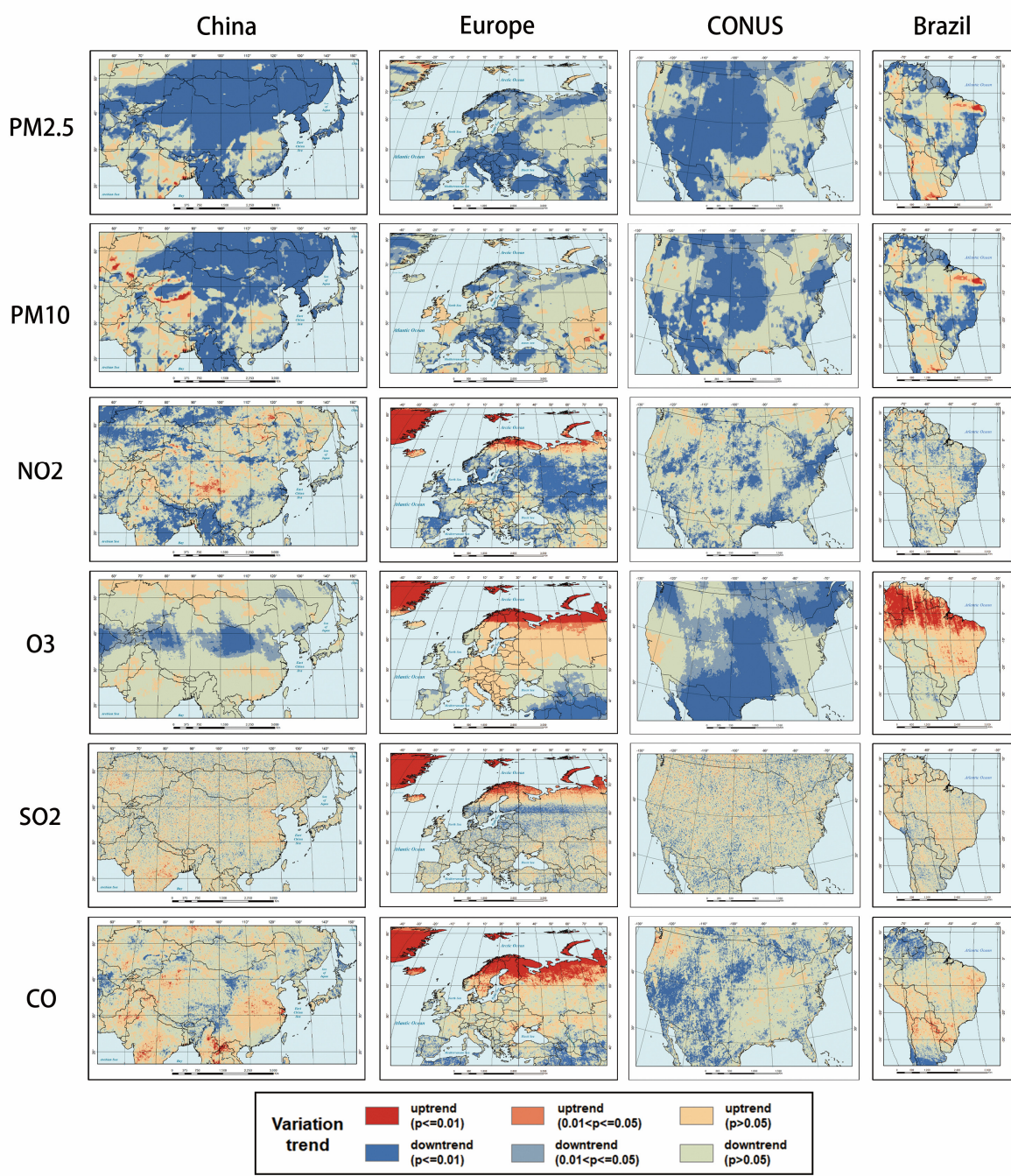
676

677

678

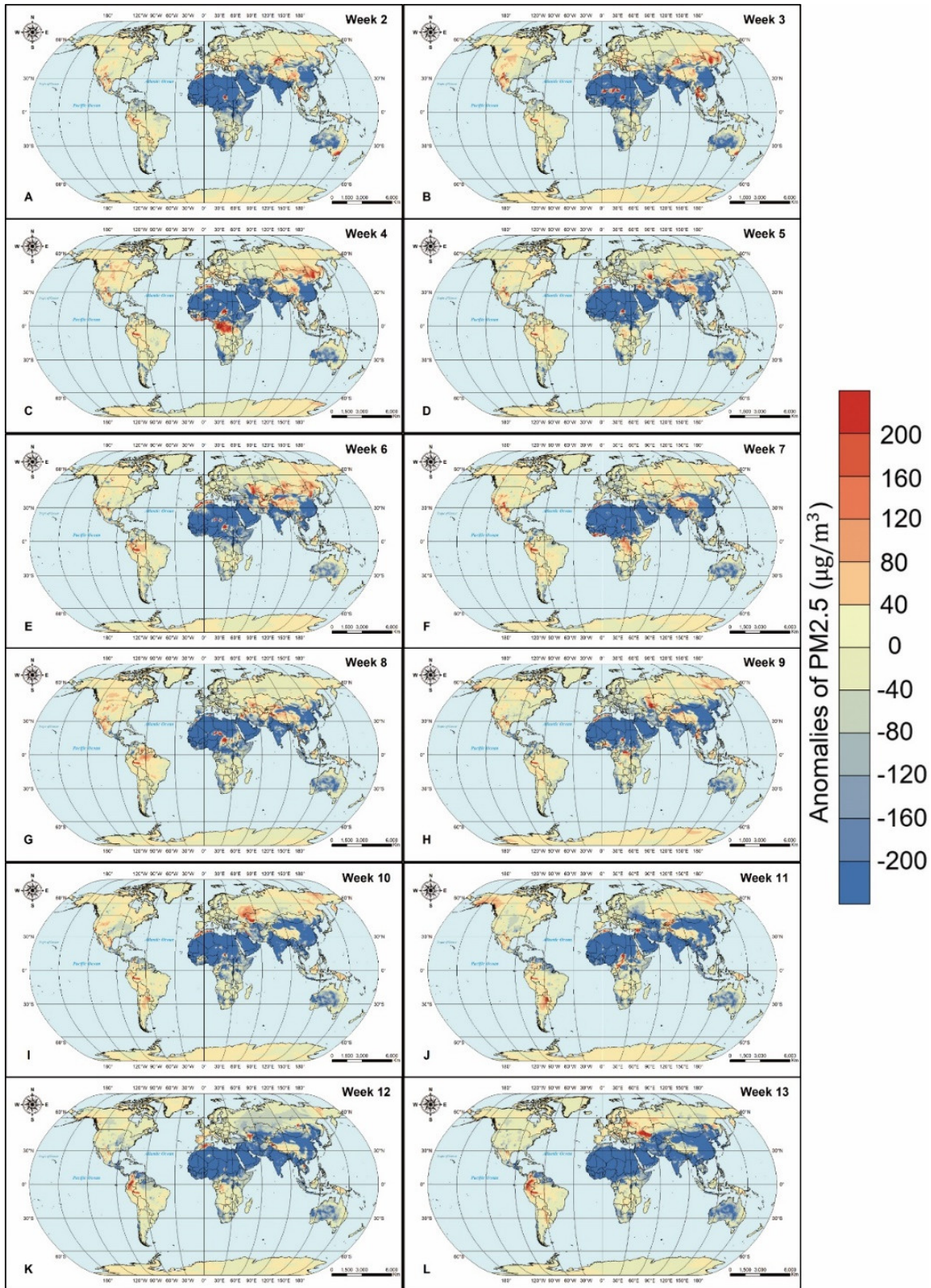
679

**Figure S2.** The v-component wind speed (VWS) in Qinghai-Tibet Plateau. A-C represent VWS for Jan. 2020 to Mar. 2020, respectively.



680  
681  
682  
683  
684

**Figure S3.** Variation trends for six pollutants anomalies in China, Europe, and CONUS. Each column represents a country, and each row represents a pollutant. All trends and significances were calculated by MK test.

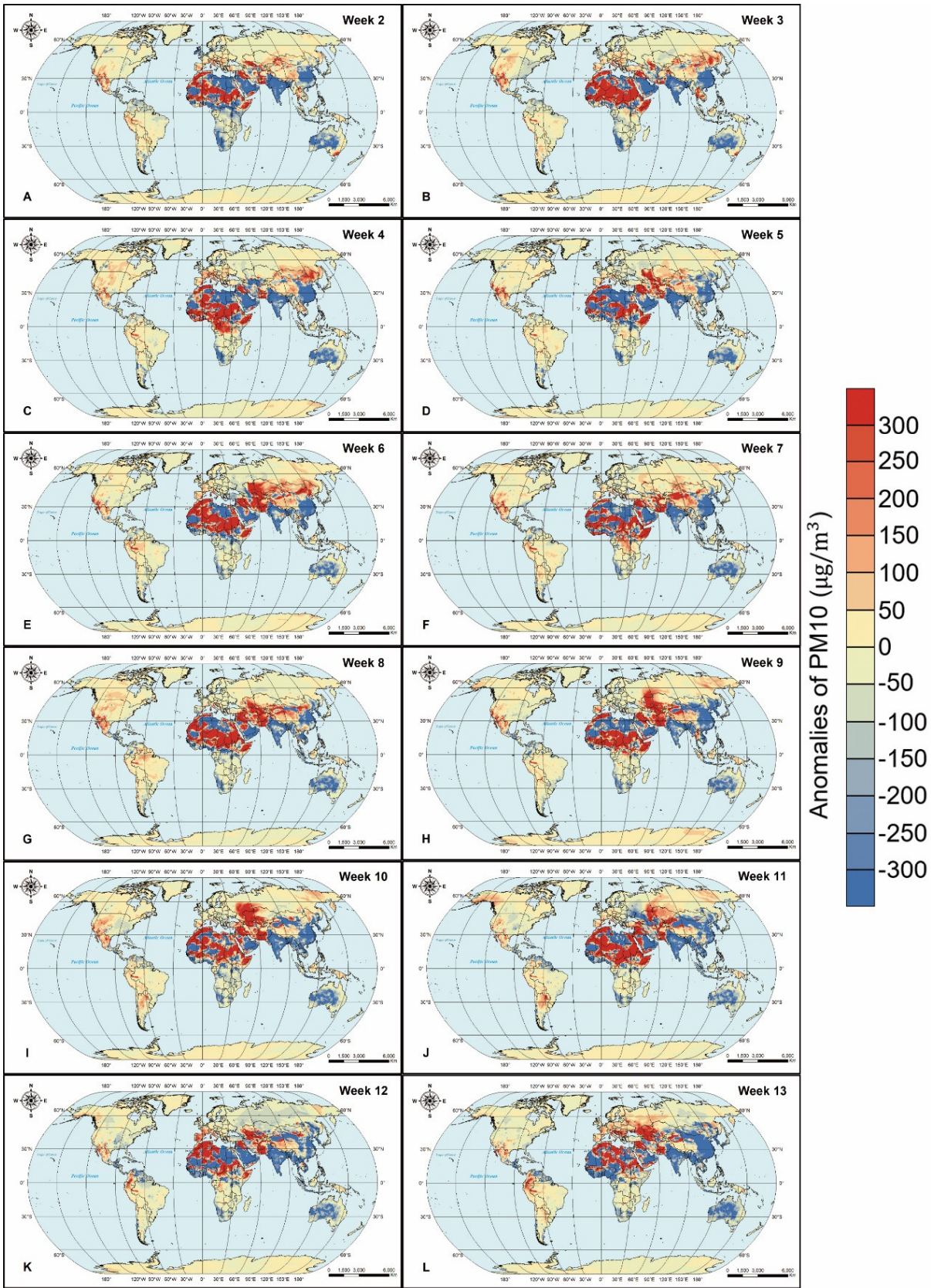


685

686

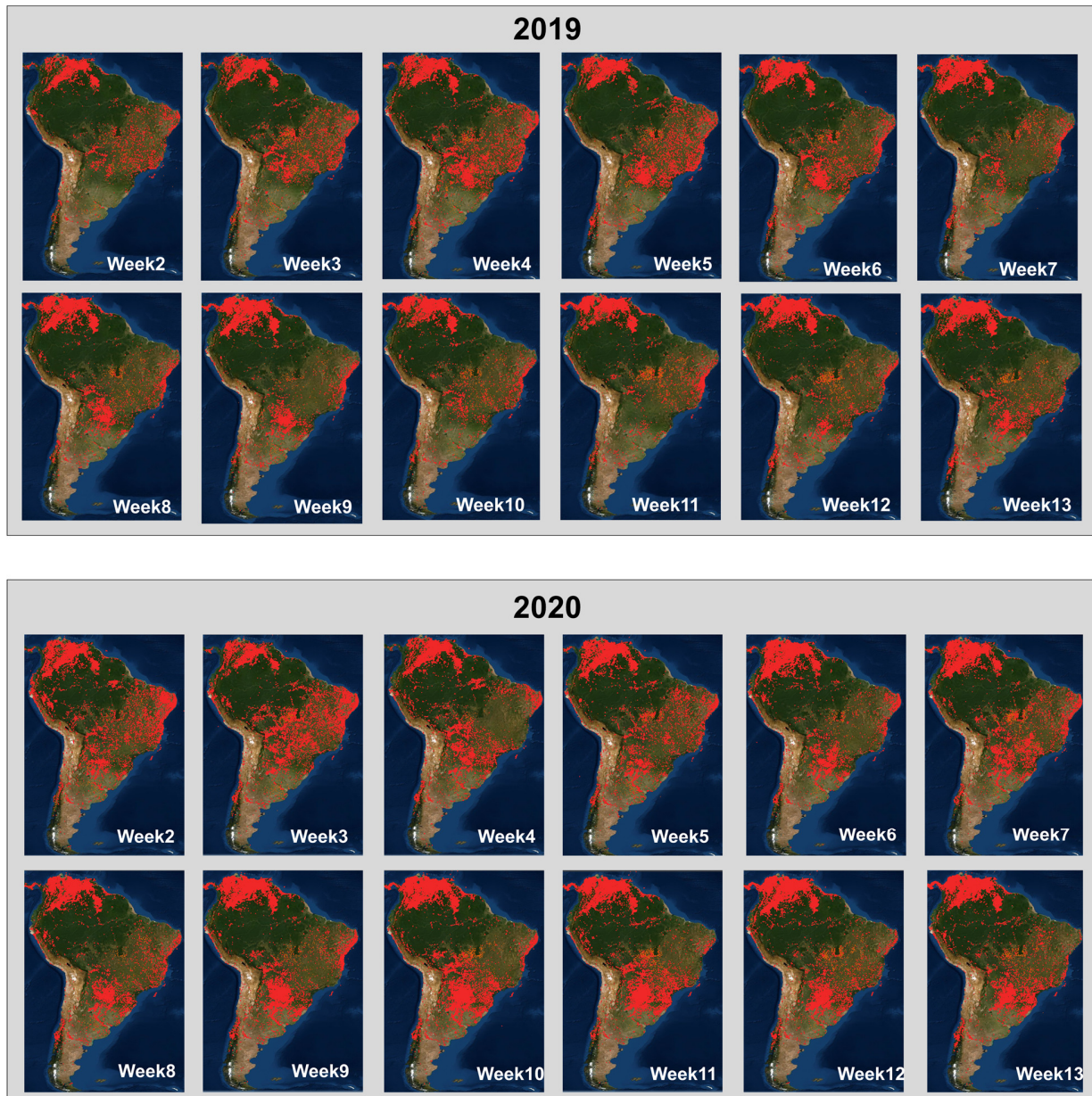
687

**Figure S4.** Global weekly averaged values of PM<sub>2.5</sub> anomalies. (A-L) represent the results in different weeks since Jan. 1, 2020.

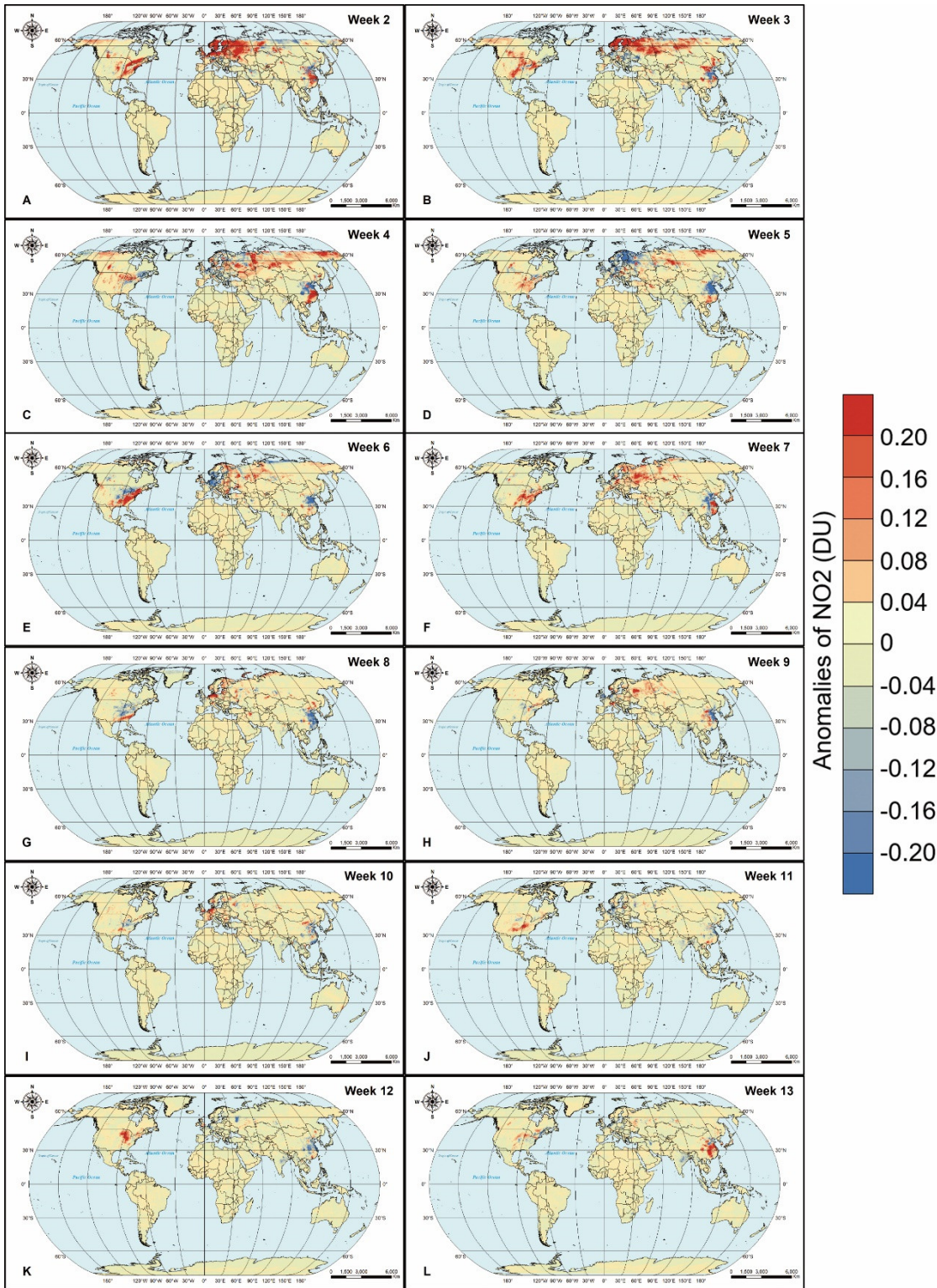


688  
689  
690  
691  
692

**Figure S5.** Global weekly averaged values of PM<sub>10</sub> anomalies. (A-L) represent the results in different weeks since Jan. 1, 2020.



693  
 694 **Figure S6.** Global weekly averaged fire data for 2019 and 2020. The data were provided by Fire  
 695 Information for Resource Management System  
 696 (<https://firms.modaps.eosdis.nasa.gov/map/#d:2020-10-17..2020-10-18;@0.0,0.0,3z>)  
 697  
 698



699

700

701

702

**Figure S7.** Global weekly averaged values of NO<sub>2</sub> anomalies. (A-L) represent the results in different weeks since Jan. 1, 2020.

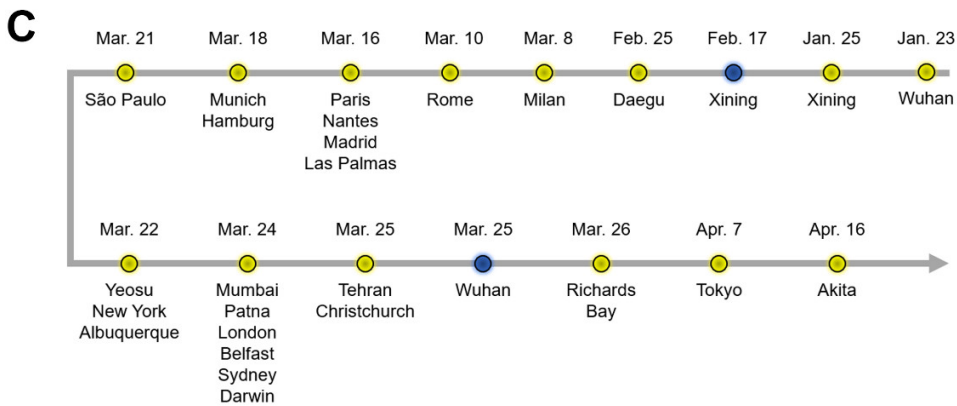
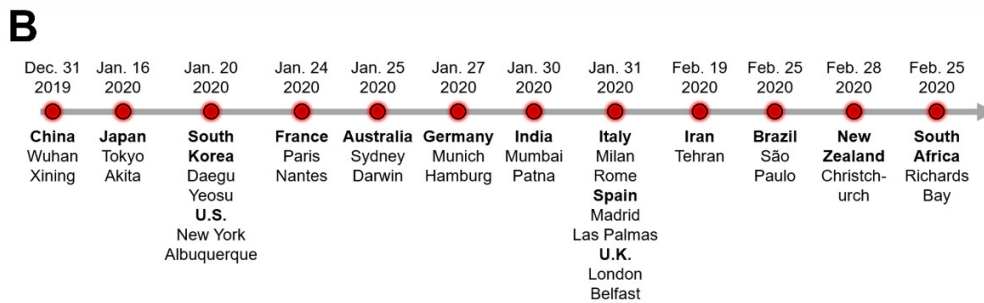
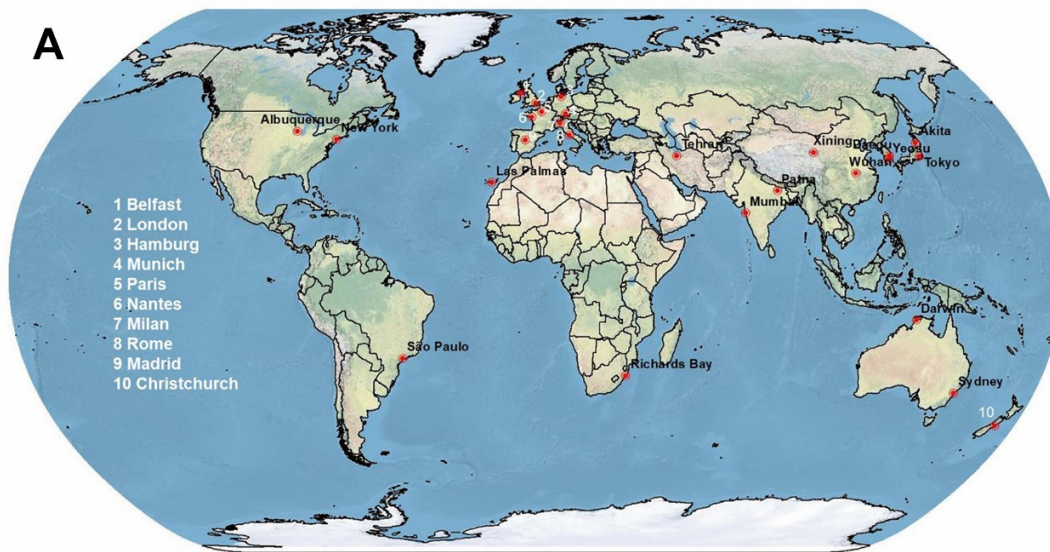


**Figure S8.** Distribution of the selected cities and their FCC time and lockdown time. (A) The spatial distribution of selected 26 cities. Cities in Europe and New Zealand are numbered to avoid congestion and the numbers for cities are on the left side of the map. (B) Times when the first case was confirmed in each city and its country (bold). (C) Times when the government declare a lockdown or other equivalent restrictions of each city. Especially, for two cities in China, we display their resumption time additionally, which were represented by blue point.

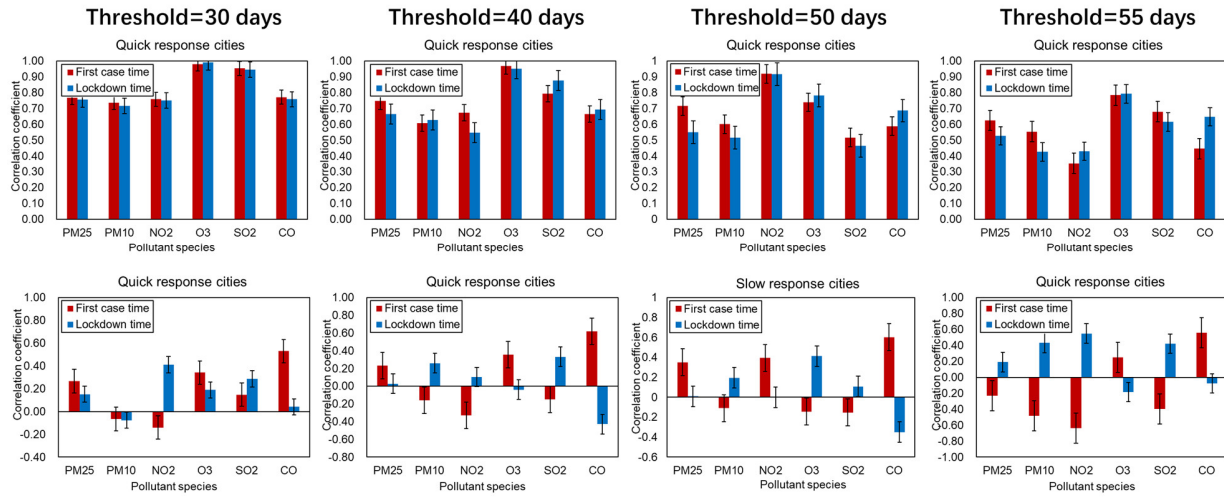


**Figure S9.** The parameter sensitivity test results for determining the number of days to differentiate slow- and quick-response cities. We set the threshold as 30 days, 40 days, 50 days, 55 days respectively to distinguish the quick- and slow-response cities, and then observed the correlation between change point and FCC/lockdown time in two group of cities. Then we found the conclusion can be relatively steady with the thresholds changing. The threshold was not set as 60 days because under this case the number of slow-response cities can be too small to analyze.

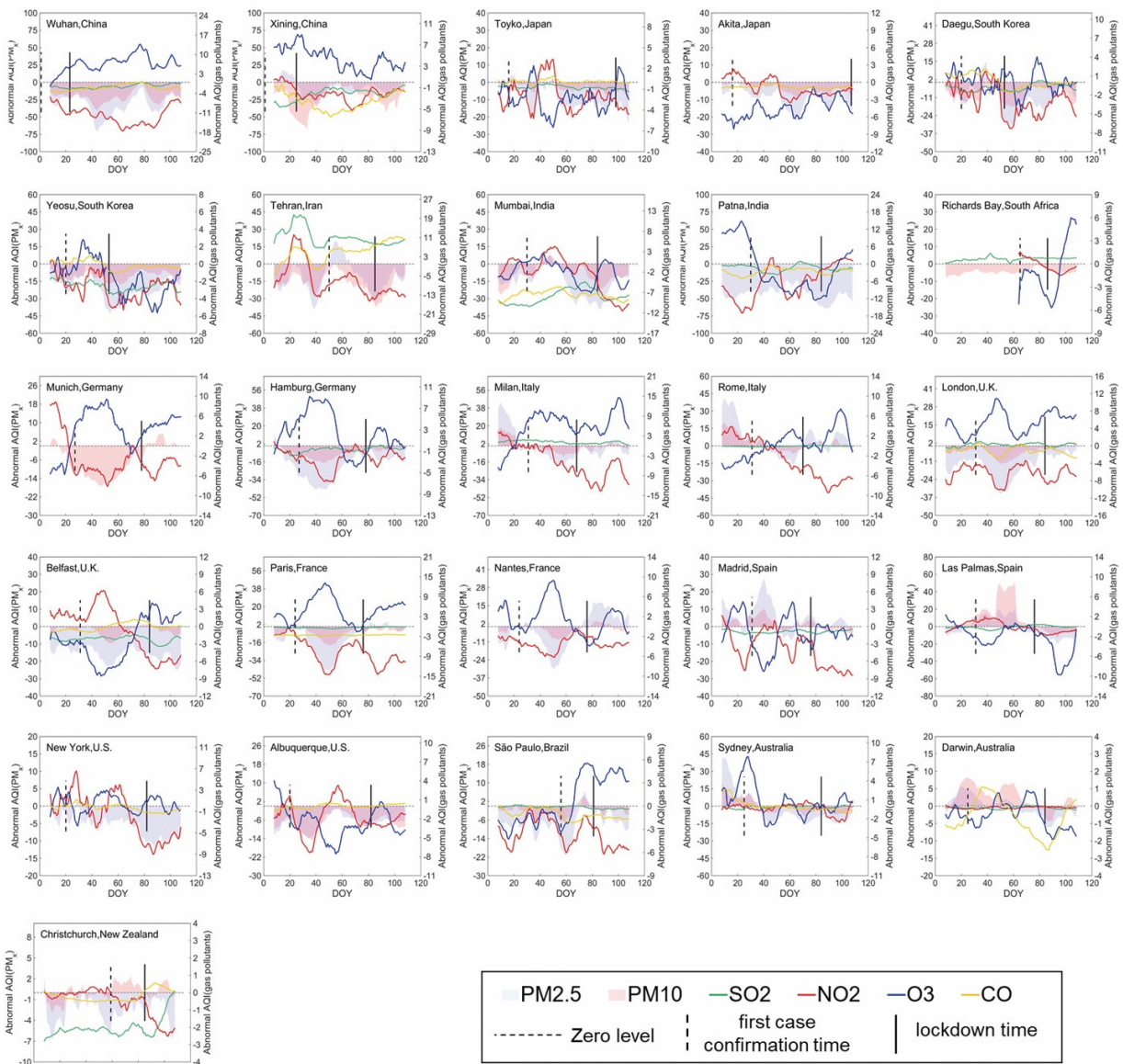
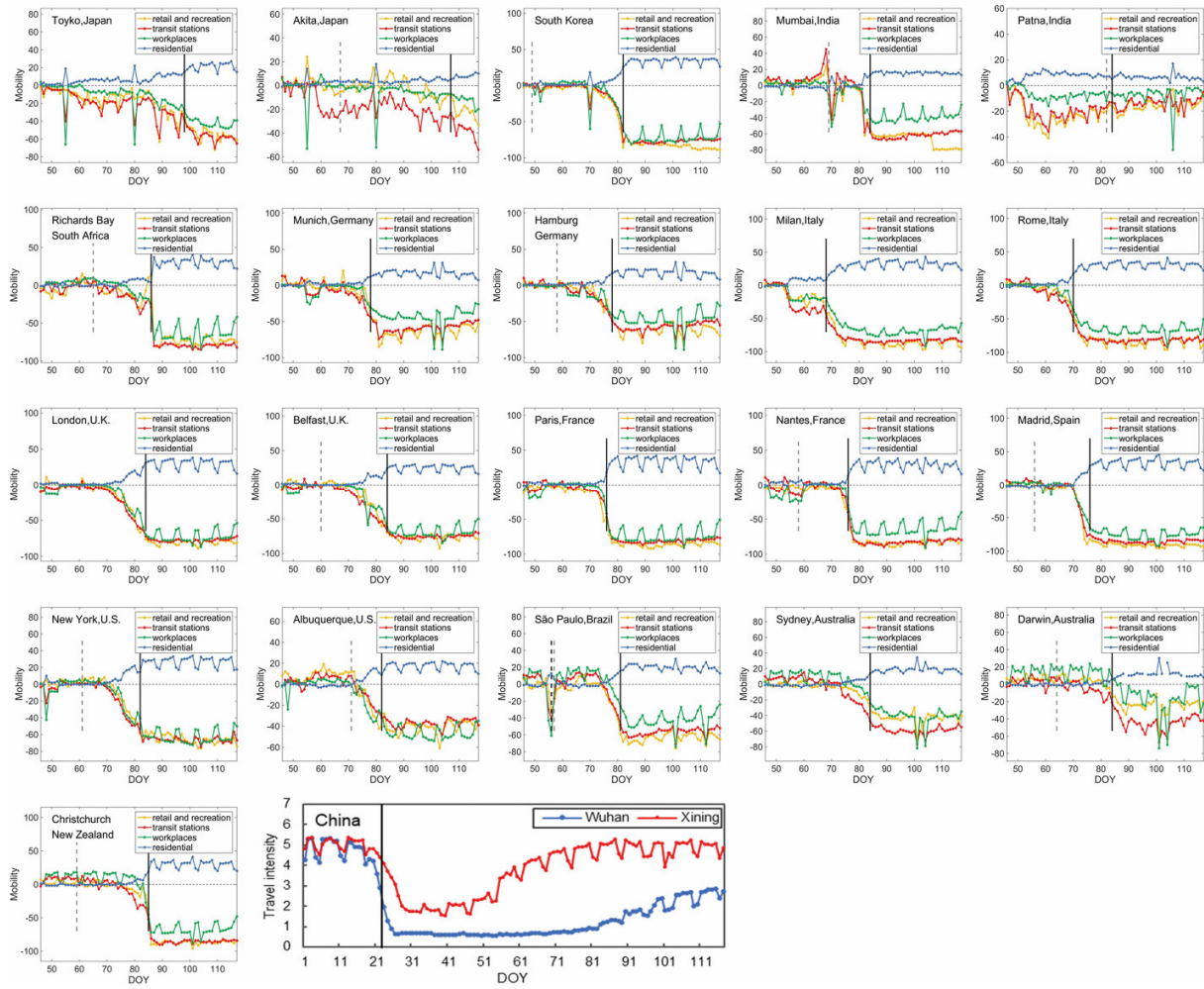
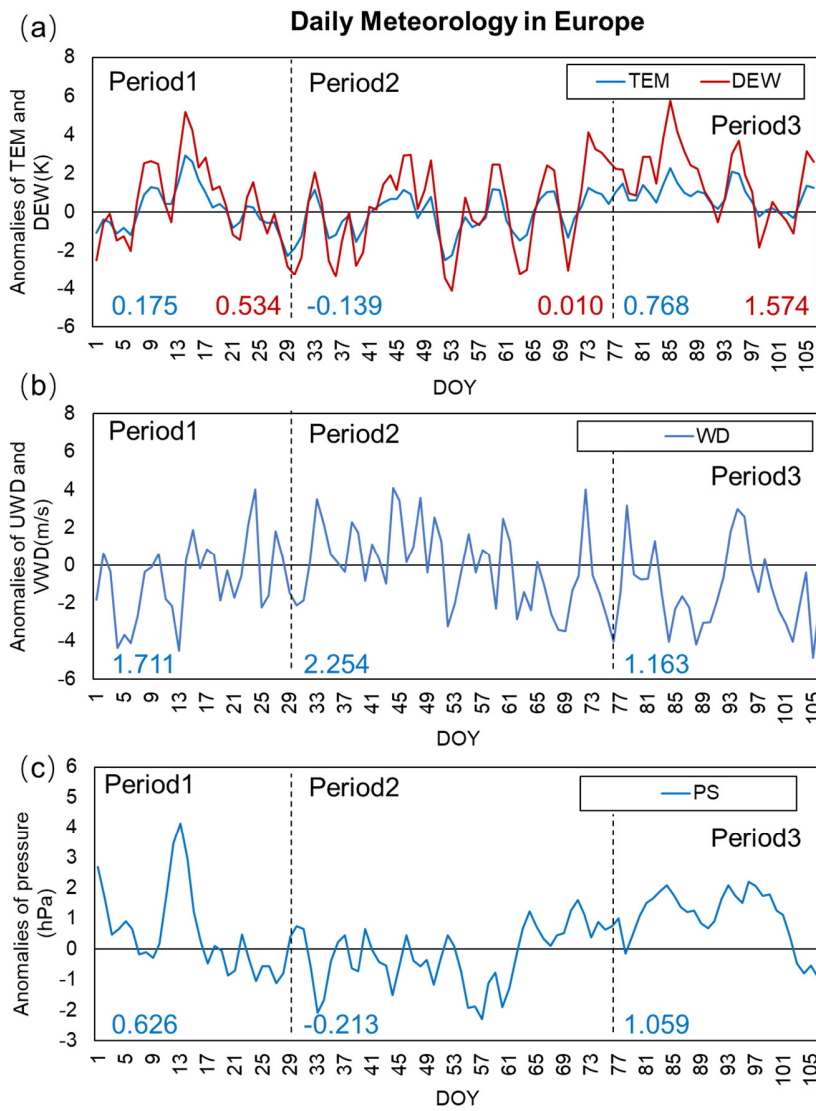


**Figure S10.** 15-day moving average trend of abnormal AQI data of six pollutants in 26 cities. The dashed vertical lines represent the first case confirmation time and the solid vertical lines represent lockdown time. The horizontal dashed lines are the  $y=0$  lines, which indicate no change of AQI.



732  
 733 **Figure S11.** Time series of mobility data in 21 cities and the intra-city travel intensity data for two  
 734 cities in China. In the first 21 subgraphs, the yellow lines, red lines, green lines, and blue lines  
 735 represent the mobility variation of retail and recreation, transit stations, workplaces, and residential,  
 736 respectively. While in the last subgraph, the blue and red lines represent the intra-city travel  
 737 intensity variations in Wuhan and Xining, respectively. The black and grey dashed vertical lines  
 738 represent the first case confirmation time of the country and of local region, the solid vertical lines  
 739 represent lockdown time. If the confirmation time or lockdown time is beyond the period of Feb.  
 740 15 to Apr. 24 then it was not displayed in the figure.  
 741  
 742



743  
744  
745  
746  
747

**Figure S12.** The daily variations of meteorological anomalies in 2020 in Europe. The blue and red numbers represent the mean values of the corresponding meteorological parameter in each period. The dashed black lines represent the mean FCC and lockdown time of the Europe cities.

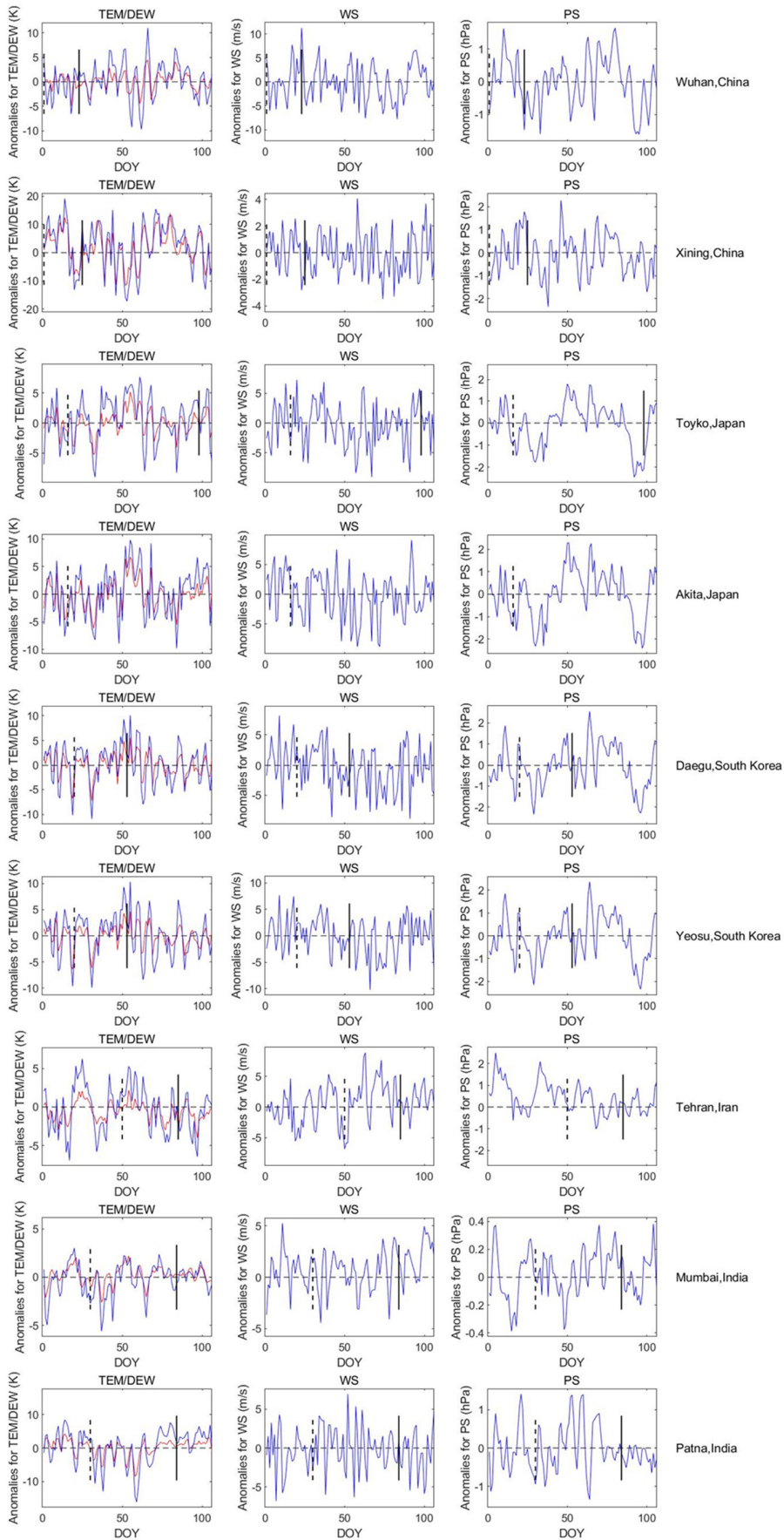


**Figure S13(1).** The daily variations of meteorological anomalies in 2020 in the 26 cities—part 1.

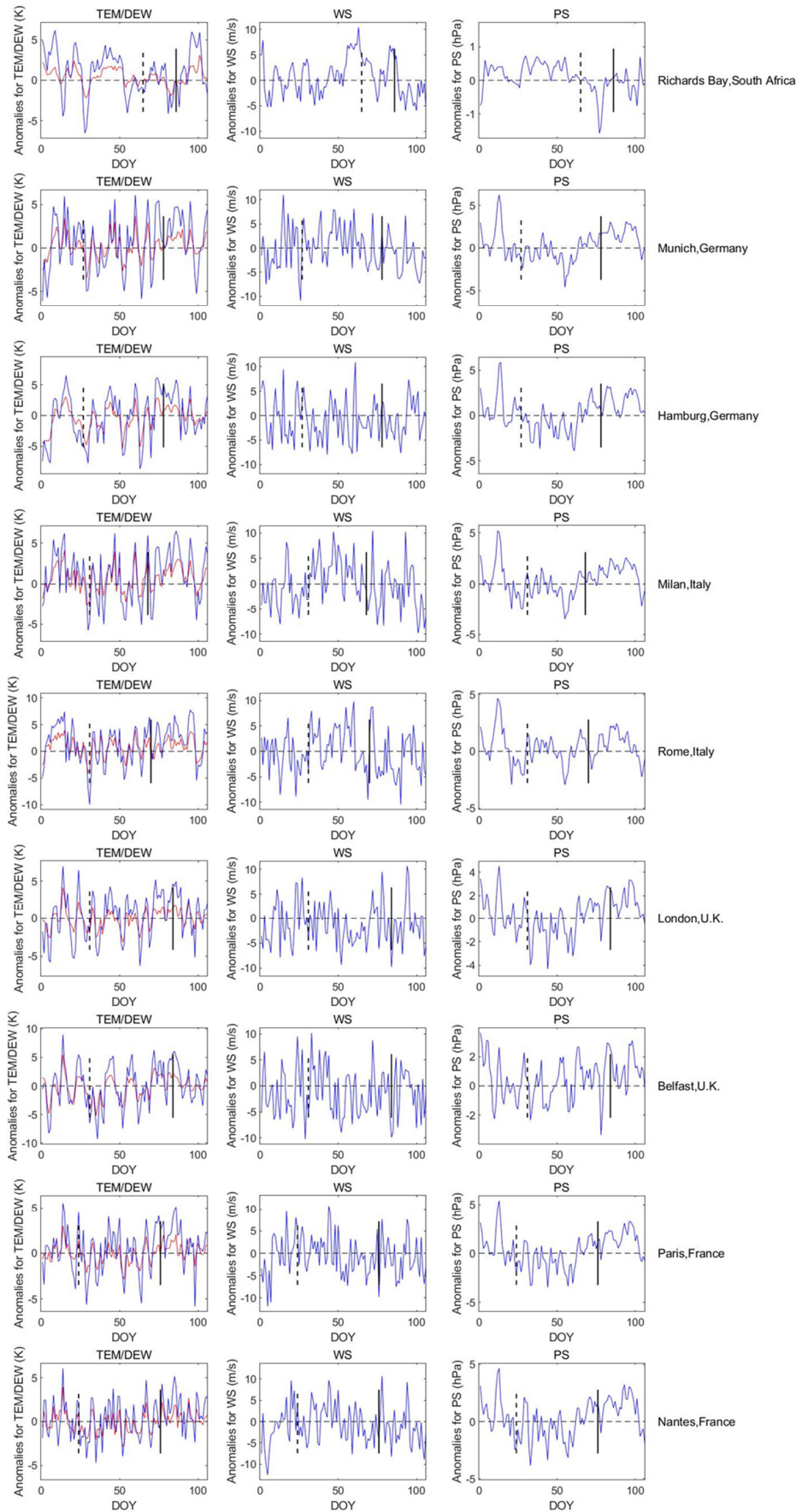


**Figure S13(2).** The daily variations of meteorological anomalies in 2020 in the 26 cities—part 2.

750  
751

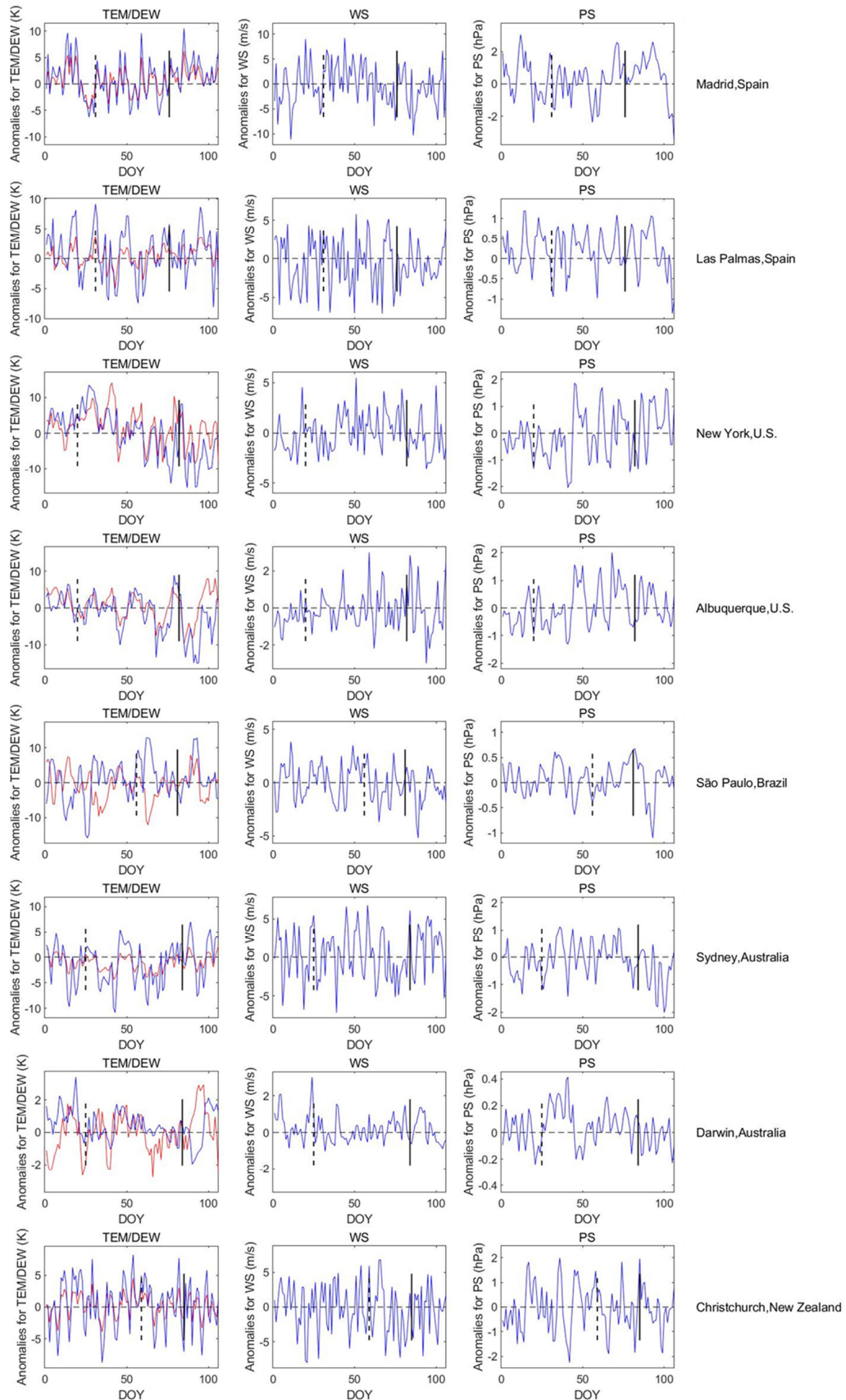
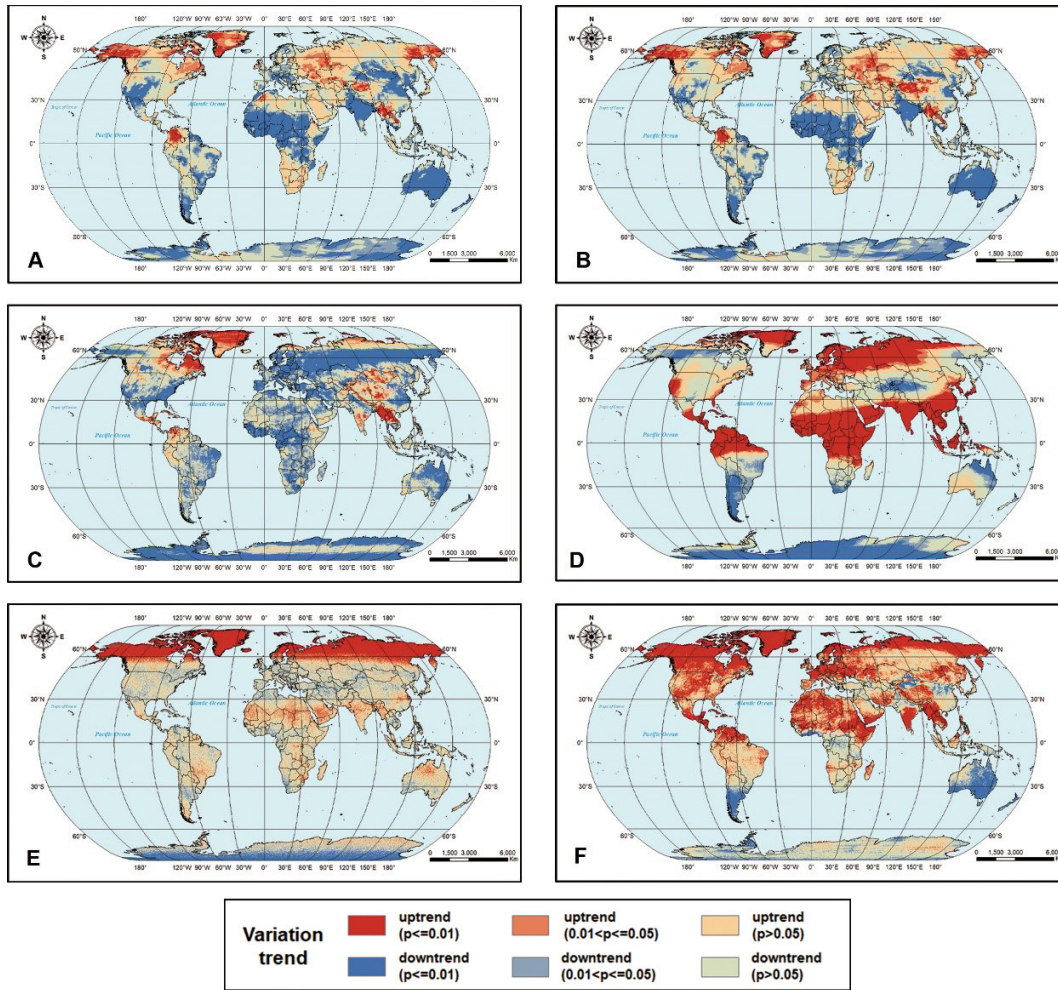


**Figure S13(3).** The daily variations of meteorological anomalies in 2020 in the 26 cities—part 3.

752  
753  
754



755

756 **Figure S14.** Global variation trends and significances of six pollutants during COVID-19. (A-L)  
 757 represents variation trends and significances of original observations of PM<sub>2.5</sub>, PM<sub>10</sub>, NO<sub>2</sub>, O<sub>3</sub>, SO<sub>2</sub>,  
 758 and CO, respectively. All results were calculated by MK test.

759

760 **Supplemental Tables**

761

762 **Table S1.** The percent of AQI change after FCC/lockdown (per1/per2) for six pollutants in 26 cities.

763 Cities above the dashed line are quick-response cities, and cities below the dashed line are slow-

764 response cities.

City	PM <sub>2.5</sub>		PM <sub>10</sub>		SO <sub>2</sub>		NO <sub>2</sub>		O <sub>3</sub>		CO	
	per1	per2	per1	per2	per1	per2	per1	per2	per1	per2	per1	per2
Richards Bay	NaN	-79.07%	25.72%	-21.65%	9.23%	1.28%	NaN	-58.36%	NaN	25.65%	NaN	NaN
Wuhan	NaN	-6.44%	NaN	-7.63%	NaN	2.91%	NaN	-36.35%	NaN	83.92%	NaN	20.73%
Xining	NaN	-22.19%	NaN	-61.64%	NaN	15.58%	NaN	-16.87%	NaN	-3.53%	NaN	-15.43%
São Paulo	4.13%	-3.40%	14.42%	-14.83%	4.46%	-37.84%	-4.81%	-23.67%	26.15%	13.32%	-28.90%	0.39%
Christchurch	-4.88%	-1.13%	12.84%	-13.66%	110.01%	290.37%	-32.54%	-75.10%	NaN	NaN	-7.24%	29.93%
Tehran	20.14%	-18.52%	4.74%	-9.46%	-8.10%	-7.06%	-9.49%	-11.58%	NaN	NaN	18.97%	16.86%
Daegu	5.79%	-19.76%	-1.18%	-4.37%	-4.03%	6.88%	2.00%	-22.56%	-13.69%	3.51%	4.40%	-26.76%
Milan	-21.94%	6.28%	-25.42%	9.98%	-2.33%	-16.30%	-12.64%	-16.90%	131.56%	-11.74%	NaN	NaN
Rome	-30.98%	15.04%	-34.07%	5.36%	-10.73%	36.06%	-13.72%	-32.85%	58.05%	0.18%	NaN	NaN
Madrid	0.82%	-19.22%	-6.24%	-27.96%	-0.99%	-1.41%	1.92%	-31.10%	-29.79%	10.49%	NaN	NaN
Las Palmas	53.67%	-43.06%	80.83%	-55.17%	0.10%	15.57%	16.55%	-31.78%	-8.03%	-9.05%	NaN	NaN
Munich	NaN	NaN	-44.87%	128.57%	NaN	NaN	-44.66%	-1.43%	112.43%	1.30%	NaN	NaN
Hamburg	-55.32%	46.22%	-55.25%	52.00%	10.76%	20.77%	-17.40%	3.69%	23.69%	-11.82%	NaN	NaN
Paris	-18.66%	54.37%	-12.34%	30.05%	-7.03%	39.55%	-32.95%	-14.54%	38.12%	-6.38%	-30.60%	212.88%
Nantes	1.17%	72.18%	-1.79%	31.19%	NaN	NaN	-20.94%	4.55%	2.39%	-13.57%	NaN	NaN
London	-16.70%	48.25%	-15.92%	43.53%	17.54%	-10.44%	-0.76%	-7.37%	23.99%	13.64%	-2.16%	-14.94%
Belfast	-2.90%	-20.81%	-5.61%	-2.04%	11.44%	-76.57%	-6.11%	-44.68%	-18.22%	47.18%	94.54%	-5.47%
Mumbai	-0.94%	-4.50%	10.19%	-10.53%	62.07%	-29.18%	6.50%	-57.08%	-3.43%	-0.79%	15.06%	-22.27%
Patna	0.56%	-12.33%	NaN	NaN	-18.13%	-3.45%	179.71%	45.60%	-103.96%	99.72%	19.48%	-11.42%
Sydney	-57.17%	-13.61%	-43.07%	-12.52%	18.97%	-7.02%	3.07%	-6.75%	-10.72%	-7.35%	-49.83%	-18.77%
Darwin	-14.32%	-31.23%	18.69%	-31.15%	3.95%	-34.88%	-16.85%	8.95%	2.65%	-30.21%	23.27%	-14.09%
Yeosu	0.30%	-19.26%	-13.84%	0.65%	-8.21%	-12.76%	-4.86%	-19.95%	2.79%	-12.22%	4.04%	-16.24%
New York	-4.81%	-15.53%	NaN	NaN	NaN	NaN	1.48%	-37.12%	-1.99%	1.95%	7.97%	-35.68%
Albuquerque	28.13%	3.13%	23.45%	5.24%	NaN	NaN	9.08%	-6.94%	-31.31%	9.83%	30.54%	13.00%
Toyko	-24.44%	-19.74%	-31.41%	-34.00%	-9.00%	-18.40%	-2.78%	-11.48%	-7.09%	10.12%	-2.99%	-3.67%
Akita	-9.55%	-32.58%	-48.61%	-72.12%	NaN	NaN	-26.70%	-3.57%	5.53%	-5.32%	5.81%	2.61%

765

766

767  
768

**Table S2.** Correlation between detected change point in time series and time of first case confirmation and lockdown.

		First-case-confirmation time		Lockdown time	
		r	p	r	p
All cities	PM <sub>2.5</sub>	0.53*	0.01	0.26	0.21
	PM <sub>10</sub>	0.41*	0.04	0.28	0.19
	SO <sub>2</sub>	0.23	0.29	0.46*	0.03
	NO <sub>2</sub>	0.69*	0.00	0.58*	0.00
	O <sub>3</sub>	0.51*	0.01	0.56*	0.00
	CO	0.48*	0.02	0.30	0.15
Quick response cities	PM <sub>2.5</sub>	0.73*	0.01	0.57*	0.05
	PM <sub>10</sub>	0.57*	0.05	0.49	0.11
	SO <sub>2</sub>	0.54	0.07	0.48	0.11
	NO <sub>2</sub>	0.92*	0.00	0.91*	0.00
	O <sub>3</sub>	0.74*	0.01	0.80*	0.01
	CO	0.60	0.07	0.70*	0.02
Slow response cities	PM <sub>2.5</sub>	0.31	0.30	-0.01	0.97
	PM <sub>10</sub>	-0.08	0.80	0.21	0.51
	SO <sub>2</sub>	-0.38	0.25	0.09	0.79
	NO <sub>2</sub>	0.37	0.19	-0.01	0.97
	O <sub>3</sub>	-0.20	0.49	0.41	0.15
	CO	0.58*	0.03	-0.38	0.18

769  
770

Note: \* represents the correlation coefficient is significant at 95% significance level.

771 **Table S3.** Percent of AQI anomalies change in different continents. per<sub>1</sub> represent the percent of  
772 change after first case confirmation before lockdown; per<sub>2</sub> represent the percent of change after  
773 lockdown.

	PM <sub>2.5</sub>		PM <sub>10</sub>		NO <sub>2</sub>	
	per <sub>1</sub>	per <sub>2</sub>	per <sub>1</sub>	per <sub>2</sub>	per <sub>1</sub>	per <sub>2</sub>
<b>Asian &amp; Africa</b>	-1% (-11%, 8%)	-23% (-36%, -11%)	-8% (-25%, 10%)	-25% (-41%, -8%)	-6% (-14%, 3%)	-26% (-39%, -14%)
<b>Europe</b>	-18% (-30%, -6%)	25% (3%, 48%)	-22% (-34%, -11%)	30% (3%, 57%)	-16% (-26%, -7%)	-16% (-26%, -5%)
<b>Other regions</b>	-8% (-29%, 12%)	-10% (-19%, -1%)	5% (-16%, 27%)	-13% (-23%, -3%)	-7% (-18%, 4%)	-23% (-45%, -2%)
<b>All cities</b>	-7% (-17%, 3%)	-5% (-18%, 7%)	-7% (-19%, 6%)	-3% (-19%, 13%)	-9% (-16%, -3%)	-22% (-30%, -14%)
	O <sub>3</sub>		SO <sub>2</sub>		CO	
	per <sub>1</sub>	per <sub>2</sub>	per <sub>1</sub>	per <sub>2</sub>	per <sub>1</sub>	per <sub>2</sub>
<b>Asian &amp; Africa</b>	-20% (-50%, 10%)	22% (-3%, 48%)	3% (-15%, 22%)	-5% (-13%, 4%)	9% (3%, 15%)	-6% (-16%, 4%)
<b>Europe</b>	38% (4%, 72%)	3% (-9%, 15%)	3% (-5%, 10%)	-1% (-29%, 26%)	21% (-40%, 81%)	64% (-55%, 183%)
<b>Other regions</b>	-3% (-19%, 13%)	-2% (-16%, 11%)	9% (-1%, 17%)	-27% (-42%, -11%)	-4% (-27%, 19%)	-4% (-21%, 13%)
<b>All cities</b>	9% (-11%, 30%)	9% (-3%, 20%)	4% (-4%, 12%)	-6% (-17%, 6%)	6% (-9%, 21%)	6% (-18%, 31%)

774 \*Numbers in the brackets represent the 95% confidence intervals. The negative sign indicates a decrease and the  
775 positive sign represent the increase. Patna was removed when calculating the mean percent of change for NO<sub>2</sub> in  
776 Asia and Africa region, in that the change of NO<sub>2</sub> in Patna can be special as described in the main text. For the  
777 analysis of SO<sub>2</sub> in other regions, Christchurch was removed for the same reason. Other regions include cities in  
778 North America, South America and Australia.  
779

780 **Table S4.** Healthy effect of AQI levels.

AQI	Air Pollution Level	Health Implications	Cautionary Statement (for PM2.5)
0 - 50	Good	Air quality is considered satisfactory, and air pollution poses little or no risk	None
51 -100	Moderate	Air quality is acceptable; however, for some pollutants there may be a moderate health concern for a very small number of people who are unusually sensitive to air pollution.	Active children and adults, and people with respiratory disease, such as asthma, should limit prolonged outdoor exertion.
101-150	Unhealthy for Sensitive Groups	Members of sensitive groups may experience health effects. The general public is not likely to be affected.	Active children and adults, and people with respiratory disease, such as asthma, should limit prolonged outdoor exertion.
151-200	Unhealthy	Everyone may begin to experience health effects; members of sensitive groups may experience more serious health effects	Active children and adults, and people with respiratory disease, such as asthma, should avoid prolonged outdoor exertion; everyone else, especially children, should limit prolonged outdoor exertion
201-300	Very Unhealthy	Health warnings of emergency conditions. The entire population is more likely to be affected.	Active children and adults, and people with respiratory disease, such as asthma, should avoid all outdoor exertion; everyone else, especially children, should limit outdoor exertion.
300+	Hazardous	Health alert: everyone may experience more serious health effects	Everyone should avoid all outdoor exertion

781  
782

## Supplemental Materials and Method

### Study region for ground-based analysis.

We selected 26 different cities and analyze the Air quality index (AQI) data of six main atmospheric pollutants (PM<sub>2.5</sub>, PM<sub>10</sub>, NO<sub>2</sub>, O<sub>3</sub>, SO<sub>2</sub>, CO) from local environmental monitoring stations. The selected 26 cities included both cities with a large number of infections and a relatively small number of infections, and included both cities with strong lockdown restrictions and soft lockdown restrictions<sup>1</sup>, for comprehensive coverage of different types of cities. These cities also covered all the continents besides Antarctica. The lockdown time and the first case confirmation time were collected from online news which reported the COVID-19 pandemic progress in the world. The first case confirmation time refers to the time when the first COVID-19 case was found in the country. The lockdown time refers to the time when the government closes most of the unnecessary public places and requires residents to stay at home unless in a special circumstance or the time when the government claims an emergency.

### Data collection and preprocessing

Ground-based measurements. AQI were used for analysis. AQI aims to evaluate the healthy effect after breathing polluted air for some time (usually 24 hours). For example, the AQI value being 188 (unhealthy) means that if a person stays out for 24 hours, the AQI is 188 during those 24 hours, then the health effect is Unhealthy, which is quite different from that if the AQI reported now is 188, then the health effect is Unhealthy. More information about healthy effect of AQI levels can be found in Table S4. The algorithm that convert raw concentrations to AQIs (scale from 0 to 500) is shown as following Equation.

$$AQI_j = \frac{AQI_{Hi} - AQI_{Lo}}{BP_{Hi} - BP_{Lo}} (C_j - BP_{Lo}) + AQI_{Lo}$$

where  $AQI_j$  refers to the AQI for pollutant  $j$ , including PM<sub>2.5</sub>, PM<sub>10</sub>, SO<sub>2</sub>, NO<sub>2</sub>, O<sub>3</sub> and CO.  $C_j$  refers to the raw concentration of pollutant  $j$ ,  $BP_{Hi}$  refers to the higher threshold of concentration  $C_j$ ,  $BP_{Lo}$  refers to the lower threshold of concentration  $C_j$ ,  $AQI_{Hi}$  refers to the AQI threshold for corresponding  $BP_{Hi}$ , and  $AQI_{Lo}$  refers to the AQI threshold for corresponding  $BP_{Lo}$ .

As shown, raw concentrations and AQIs can be converted to each other theoretically. However, the raw concentrations usually cannot be calculated inversely from AQIs because the thresholds (i.e.  $BP_{Hi}$  and  $BP_{Lo}$ ) varies from country to country and often unavailable. Therefore, we calculated anomalies based on AQIs data uniformly when conducting time series analysis for ground-based data

AQI data for six main atmospheric pollutants from ground monitoring stations<sup>2</sup> was provided by the World Air Quality Index project. The project is providing transparent air quality information for more than 100 countries, covering more than 12,000 stations in 1000 major cities, via the website: <https://aqicn.org/>. All the Air Quality data seen on World Air Quality Index are the official data from each country's respective Environmental Protection Agency (EPA). The AQI standard for every single published station is based on the US EPA Instant-Cast standard. Quality of the data has been controlled through a set of real-time artificial intelligent (AI) algorithms (detect abnormal data conditions such as sparks, low reporting, etc. and automatically 'disable' data reported from defective stations.). Historical air quality data were provided on the database platform page (<https://aqicn.org/data-platform/register/>) and real-time air quality data can be accessed using the API (<https://aqicn.org/api/>). Recently, this website has also published AQI data for cities in the world, and data was given in the form of max value, min value, median, and variance. The median data was used to represent the AQI level in the city in this study. Then data for the 26 selected cities were extracted. The study period of ground station measurements was from 1 January to 24 April 2020.

829 We deleted abnormal values (such as zero value, negative value, etc.) in the original time series  
830 data. After data quality check and filtering, for most of the 26 selected cities, there were six kinds  
831 of pollutants available, and for other cities, data for some kinds of pollutants are missing. We listed  
832 cities which the data are lacked for each kind of pollutant below:

- 833 • PM<sub>2.5</sub>: Munich
- 834 • PM<sub>10</sub>: Patna, New York
- 835 • NO<sub>2</sub>: \
- 836 • O<sub>3</sub>: Tehran, Christchurch
- 837 • SO<sub>2</sub>: Akita, Munich, Nantes, New York
- 838 • CO: Christchurch, Munich, Hamburg, Milan, Rome, Nantes, Madrid, Las Palmas

839 Satellite observations and reanalysis data. The study period of satellite observations and  
840 reanalysis data was from 1 January to 31 March 2020. The concentration data for four kinds of gas  
841 pollutants (NO<sub>2</sub>, O<sub>3</sub>, SO<sub>2</sub>, CO) were obtained from TROPospheric Monitoring Instrument  
842 (TROPOMI) and Ozone Monitoring Instrument (OMI); the PM<sub>2.5</sub> and PM<sub>10</sub> (PM<sub>x</sub>) concentration  
843 data were provided by the Copernicus Atmosphere Monitoring Service (CAMS) reanalysis data.

844 The Sentinel-5 Precursor (Sentinel-5P) satellite mission is one of the European Space  
845 Agency's (ESA) new mission family: Sentinels. The sensor payload on Sentinel-5P is TROPOMI<sup>3</sup>,  
846 which is a nadir-viewing 108° Field-of-View push-broom grating hyperspectral spectrometer,  
847 covering the wavelength of Ultraviolet-Visible (UV), Near Infrared (NIR), and ShortWave  
848 InfraRed (SWIR). Sentinel-5P is the first of the atmospheric composition sentinels and is expected  
849 to provide measurements of O<sub>3</sub>, NO<sub>2</sub>, SO<sub>2</sub>, etc. at high spatial, temporal, and spectral resolutions.  
850 In our study, TROPOMI products of NO<sub>2</sub>, SO<sub>2</sub>, CO, and O<sub>3</sub> in 2020 and 2019 are employed. The  
851 CO product has a spatial resolution of 0.07°×0.07°, while that of other products utilized is  
852 0.05°×0.05°. All products have the same temporal resolution of daily and were resampled to  
853 0.1°×0.1° using the bilinear interpolation.

854 OMI<sup>4</sup> employs hyperspectral imaging in a push-broom mode to observe solar backscatter  
855 radiation in the visible and UV bands, which is onboard the Aura satellite. The Earth will be viewed  
856 in 740 wavelength bands along the satellite track with a swath large enough to provide global  
857 coverage in 14 orbits (1-day). OMI will continue the Total Ozone Mapping Spectrometer (TOMS)  
858 record for O<sub>3</sub> and other atmospheric parameters related to O<sub>3</sub> chemistry and climate, including NO<sub>2</sub>,  
859 formaldehyde (HCHO), and aerosol characteristics. In our study, OMI products of NO<sub>2</sub> and O<sub>3</sub>,  
860 whose spatial resolution are 0.25°×0.25° and temporal resolution are daily, in 2017 and 2018 are  
861 collected and resampled to 0.1°×0.1° using the bilinear interpolation. The units for all the satellite  
862 data are unified into DU.

863 CAMS reanalysis<sup>5</sup> is the latest global reanalysis dataset of atmospheric composition, including  
864 aerosols and atmospheric chemical species. The dataset builds on the experience gained during the  
865 production of the earlier Monitoring Atmospheric Composition and Climate (MACC) reanalysis  
866 and CAMS interim reanalysis. CAMS reanalysis can provide surface-level products of atmospheric  
867 compositions (e.g. NO<sub>2</sub> and PM<sub>x</sub>) at a high temporal resolution (3-hour) but relatively low spatial  
868 resolution (0.8°×0.8°), which are gridded data sets constructed by blending satellite observations  
869 with model simulations. In our study, CAMS products of PM<sub>2.5</sub> and PM<sub>10</sub> are utilized and resampled  
870 to 0.1°×0.1° using the bilinear interpolation and averaged to daily.

871 The global meteorological data were also provided by CAMS, with a 3-hour and 0.4°×0.4°  
872 resolution. We selected 6 commonly used meteorological variables for analysis, including:  
873 temperature (full name in the product: 2m temperature, abbreviation in the manuscript: TEM),  
874 dewpoint temperature (2m dewpoint temperature, DEW), zonal wind (10m u-component of wind,

UWS), meridional wind (10m v-component of wind, VWS), precipitation (large-scale precipitation, PRE), and pressure (mean sea-level pressure, PS). The 3-h data was averaged to the daily data for analysis in this study. When analyzing the meteorological conditions for specific city, the pixels within the bounding rectangle of the city's administrative boundary were averaged to represent the meteorological condition of the city. The anomalies and the change of meteorological factor in different periods were calculated using the same method as the ground based AQI data. The composite wind speed was calculated from the zonal wind speed and meridional wind speed using the following equation:

$$WS = \sqrt{UWS^2 + VWS^2} .$$

Transportation data include two parts. For Chinese cities, the intra-city travel intensity data from the Baidu map (<http://qianxi.baidu.com>) was used, which can be accessed through the Application Program Interface (API) provided by Baidu. Intra-city travel intensity represents the indexed result of the ratio of the number of people traveling in the city to the city 's inhabitants, and the data is available from 1 January to 24 April 2020.

For other cities in the world, the transportation data was provided by Google Community Mobility Reports (<https://www.google.com/covid19/mobility/>), which are aimed to provide insights into what has changed in response to policies aimed at combating COVID-19 aim. The reports chart movement trends over time by geography, across different categories of places such as retail and recreation, groceries and pharmacies, parks, transit stations, workplaces, and residential. These categories are divided based on google map and the movement trends are collected by google accounts' location history data anonymously. Changes for each day are compared to a baseline value for that day of the week. The baseline is the median value, for the corresponding day of the week, during a 5-week period of 3 January to 6 February 2020. The data were provided for different regions in the world with varying spatial scales. For example, for Korea, the data were provided in the unit of the country, that's to say, there is only one data for one day in the country. For Italy, the data were provided in the unit of Region, such as Lombardia and Lazio. For Japan, the data were provided in the unit of the city, such as Tokyo and Akita. Overall, for most areas, the data were provided in the unit of first-level administrative division in each country. Since we mainly studied the air quality change in city-scale when analyzing the ground-based data, the Google mobility data were also matched with our selected 26 cities. We represent the mobility in the city using mobility data of the region where it belongs. The data was accessible since 15 February 2020. Since start date can be later than the time of the first case confirmation in most countries, when calculating the contribution of the first case confirmation and lockdown to the mobility data decrease, we utilized the first case confirmation time of local region rather than of the whole country.

### Processing of missing data

We usually calculated averaged measurements of previous three years as baseline when conducting time series analysis for satellite and reanalysis data. But for SO<sub>2</sub> and CO data, only data from 2019 were used to calculate anomalies for the lack of data in 2017 and 2018.

Ground-based dataset also has missing part. For Tehran, Iran, data of 2017 was lacking, and only data in 2018 and 2019 were used as baseline; for PM<sub>2.5</sub>, NO<sub>2</sub> and O<sub>3</sub> AQI data in Richards Bay, South Africa, data in 2017 and 2018 were lacking, and only data in 2019 were used as a baseline.

## Supplemental References

1. COVID-19 pandemic by country and territory in Wikipedia [https://en.wikipedia.org/wiki/COVID-19\\_pandemic\\_by\\_country\\_and\\_territory](https://en.wikipedia.org/wiki/COVID-19_pandemic_by_country_and_territory) [accessed 18 May 2020]
2. Wang, Y., Ying, Q., Hu, J., and Zhang, H. (2014). Spatial and temporal variations of six criteria air pollutants in 31 provincial capital cities in China during 2013–2014. *Environ. Int.* *73*, 413–422.
3. Veefkind, J.P., Aben, I., McMullan, K., Förster, H., de Vries, J., Otter, G., Claas, J., Eskes, H.J., de Haan, J.F., Kleipool, Q., et al. (2012). TROPOMI on the ESA Sentinel-5 Precursor: A GMES mission for global observations of the atmospheric composition for climate, air quality and ozone layer applications. *Remote Sens. Environ.* *120*, 70–83.
4. Levelt, P.F., Oord, G.H.J. van den, Dobber, M.R., Malkki, A., Visser, H., Vries, J. de, Stammes, P., Lundell, J.O. V, and Saari, H. (2006). The ozone monitoring instrument. *IEEE Trans. Geosci. Remote Sens.* *44*, 1093–1101.
5. Inness, A., Ades, M., Agustí-Panareda, A., Barré, J., Benedictow, A., Blechschmidt, A.-M., Dominguez, J.J., Engelen, R., Eskes, H., Flemming, J., et al. (2019). The CAMS reanalysis of atmospheric composition. *Atmos. Chem. Phys.* *19*, 3515–3556.